SARS-CoV-2 B.1.617.2 Delta variant emergence, replication and sensitivity to neutralising antibodies

Petra Mlcochova[1,2]*, Steven Kemp[1,2,6]*, Mahesh Shanker Dhar[3]*, Guido Papa[4], Bo Meng[1,2], Swapnil Mishra[5], Charlie Whittaker[5], Thomas Mellan[5], Isabella Ferreira[1,2], Rawlings Datir[1,2], Dami A. Collier[,2,6], Anna Albecka[4], Sujeet Singh[3], Rajesh Pandey[7], Jonathan Brown[8], Jie Zhou[8], Niluka Goonawardne[8], Robin Marwal[3], Meena Datta[3], Shantanu Sengupta[7], Kalaiarasan Ponnusamy[3], Venkatraman Srinivasan Radhakrishnan[3], Adam Abdullahi[1,2], Oscar Charles[6], Partha Chattopadhyay[7], Priti Devi[7], Daniela Caputo[9], Tom Peacock[8], Dr Chand Wattal[10], Neeraj Goel[10], Ambrish Satwik[10], Raju Vaishya[11], Meenakshi Agarwal[12], The Indian SARS-CoV-2 Genomics Consortium (INSACOG), The CITIID-NIHR BioResource COVID-19 Collaboration, The Genotype to Phenotype Japan (G2P-Japan) Consortium, Antranik Mavousian[13], Joo Hyeon Lee[13,14], Jessica Bassi[15] , Chiara Silacci-Fegni[15], Christian Saliba[15], Dora Pinto[15] , Takashi Irie[16], Isao Yoshida[17], William L. Hamilton[2], Kei Sato[18,19], Leo James[4], Davide Corti[15], Luca Piccoli[15], Samir Bhatt[4,20,], Seth Flaxman[21], Wendy S. Barclay[8], Partha Rakshit[3*], Anurag Agrawal[7*], Ravindra K. Gupta[1,2, 22*]

[1] Cambridge Institute of Therapeutic Immunology & Infectious Disease (CITIID), Cambridge, UK.

[2] Department of Medicine, University of Cambridge, Cambridge, UK.

[3] National Centre for Disease Control, Delhi, India

[4] MRC – Laboratory of Molecular Biology, Cambridge, UK.

[5] Medical Research Council (MRC) Centre for Global Infectious Disease Analysis, Jameel Institute, School of Public Health, Imperial College London, UK.

[6] University College London, London, UK

[7] CSIR Institute of Genomics and Integrative Biology, Delhi, India

[8]Department of Infectious Diseases, Imperial College London, UK.

[9] NIHR Bioresource, Cambridge, UK

[10] Sri Ganga Ram Hospital, New Delhi, India

[11] Indraprastha Apollo Hospital, New Delhi

[12] Northern Railway Central Hospital, New Delhi, India

[13] Wellcome-MRC Cambridge Stem Cell Institute, Cambridge, UK.

[14]Department of Physiology, Development and Neuroscience, University of Cambridge, Cambridge, UK.

[15]Humabs Biomed SA, a subsidiary of Vir Biotechnology, 6500 Bellinzona, Switzerland
[16] Institute of Biomedical and Health Sciences, Hiroshima University, Hiroshima 7348551, Japan
[17] Tokyo Metropolitan Institute of Public Health, Tokyo 1690073, Japan
[18] Division of Systems Virology, The Institute of Medical Science, The University of Tokyo, Tokyo 1088639, Japan
[19] CREST, Japan Science and Technology Agency, Saitama 3220012, Japan
[20] Section of Epidemiology, Department of Public Health, University of Copenhagen, Denmark
[21] Department of Mathematics, Imperial College London, London, UK
[22]Africa Health Research Institute, Durban, South Africa.

*Authors contributed equally to this work
Address for correspondence:
rkg20@cam.ac.uk; a.agrawal@igib.in; partho_rakshit@yahoo.com

Key words: SARS-CoV-2; COVID-19; B.1.617; antibody escape; neutralising antibodies; infectivity; spike mutation; evasion; resistance; fitness; Delta variant

Abstract

The SARS-CoV-2 B.1.617.2 (Delta) variant was first identified in the state of Maharashtra in late 2020 and spread throughout India, displacing the B.1.1.7 (Alpha) variant and other pre-existing lineages, including B.1.617.1 that was detected prior to B.1.617.2. Bayesian modelling indicates that the growth advantage of B.1.617.2 in Mumbai was most likely explained by increased transmissibility and immune evasion from previous infection. Indeed *in vitro*, we demonstrate that B.1.617.2 is approximately 6-fold less sensitive to neutralising antibodies in sera from recovered individuals, and approximately 8-fold less sensitive to vaccine-elicited antibodies as compared to wild type Wuhan-1 bearing D614G. B.1.617.2 spike pseudotyped viruses exhibited compromised sensitivity to monoclonal antibodies against the receptor binding domain (RBD) and N- terminal domain (NTD), in particular to the clinically approved bamvalinumb and imdevimab monoclonal antibodies. B.1.617.2 demonstrated higher replication efficiency in both airway organoid and human airway epithelial systems as compared to B.1.1.7, associated with B.1.617.2 spike being in a predominantly cleaved state compared to B.1.1.7. In an analysis of vaccinated healthcare workers across three centres in India during a period of mixed lineage circulation, we observed reduced ChAdOx-1 vaccine efficacy against B.1.617.2 relative to non- B.1.617.2. These combined epidemiological and *in vitro* data indicate that the dominance of B.1.617.2 in India has been most likely driven by a combination of evasion of neutralising antibodies in previously infected individuals and increased virus infectivity. B.1.617.2 threatens the efficacy of critically important therapeutic monoclonal antibodies for COVID-19 and compromised vaccine efficacy mandates continued infection control measures in the post-vaccination era.

Introduction

India's first wave of SARS-CoV-2 infections in mid-2020 was relatively mild and was controlled by a nationwide lockdown. Since easing of restrictions, India has seen expansion in cases of COVID-19 since March 2021 with widespread fatalities and a death toll of over 400,000. The B.1.1.7 Alpha variant, introduced by travel from the United Kingdom (UK) in late 2020, expanded in the north of India and is known to be more transmissible than previous viruses bearing the D614G spike mutation, whilst maintaining sensitivity to vaccine elicited neutralising antibodies[1,2]. The B.1.617 variant was first identified in the state of Maharashtra in late 2020/early 2021[3] , spreading throughout India and to at least 90 countries. The first sub-lineage to be detected was B.1.617.1[4-6] , followed by B.1.617.2, both bearing the L452R spike receptor binding motif mutation also observed in B.1.427/B.1.429[7]. This mutation was previously reported to confer increased infectivity and a modest loss of susceptibility to neutralising antibodies[8,9]. B.1.617.2, termed the Delta variant by WHO, has since dominated over B.1.617.1 (Kappa variant) and other lineages including B.1.1.7 globally (https://nextstrain.org/sars-cov-2)[10]. B.1.617.2 bears spike mutations T19R, G142D, E156G, F157del, R158del, L452R, T478K, D614G, P681R and D950N relative to Wuhan-1 D614G.

Although vaccines have been available since early 2021, achieving near universal coverage has in adults has been an immense logistical challenge, in particular for populous nations where B.1.617.2 is growing rapidly with considerable morbidity and mortality[11]. Current vaccines were designed to target the B.1, Wuhan-1 virus, and the emergence of variants with reduced susceptibility to vaccines such as B.1.351 and P.1 has raised fears for longer term control and protection through vaccination[12,13], particularly in risk groups[14,15]. The specific reasons behind the explosive global growth of B.1.617.2 in populations remain unclear. Possible explanations include increased infectivity as well as evasion of neutralising antibodies generated through vaccination or prior infection.

Here we analyse the growth and dominance of the B.1.617.2 Delta variant in Mumbai, with modelling analysis that implicates combined effects of immune evasion and increased transmissibility. We find significantly reduced sensitivity of B.1.617.2 to convalescent sera and sera from BNT162b and ChAdOx-1 vaccinees. Furthermore we find substantial loss of sensitivity to a large panel of spike specific monoclonal antibodies, including compromise of key monoclonals that are clinically approved - imdevimab and bamlanivumab. We show that B.1.617.2 exhibits higher replication over B.1.1.7 in two independent airway model systems

137 and that B.1.617.2 spike protein mediates more efficient cell entry and augmented syncytium
138 formation, a process implicated in severe disease. Moreover, B.1.617.2 appears to confer an
139 entry and replication advantage over B.1.617.1. In vaccinated health care workers (HCW) we
140 find evidence for reduced ChAdOx-1 efficacy against B.1.617.2 relative to non- B.1.617.2.
141 These data indicate that (i) significant immune evasion and virus fitness are both responsible
142 for the observed global dominance of B.1.617.2, (ii) that health care settings should maintain
143 infection control in settings where B.1.617.2 is prevalent and (iii) that REGN-COV2
144 combination therapy could be compromised by B.1.617.2, particularly in those with immune
145 deficiency with concomitant risk of selection of escape mutants.
146
147 **Results**
148 **B.1.617.2 growth advantage due to re-infection and increased transmissibility**
149 We plotted the relative proportion of variants in new cases of SARS-CoV-2 in India since the
150 start of 2021. Whilst B.1.617.1 emerged earlier, and co-circulated with B.1.1.7, it has since
151 been replaced by B.1.617.2, which rapidly grew to predominate sequenced infections in India
152 from March 2021 onwards (**Figure 1a**). We characterised B.1.617.2's epidemiological
153 properties through dynamical modelling of the recent resurgence of SARS-CoV-2 transmission
154 in Mumbai. We utilised a Bayesian model of SARS-CoV-2 transmission and mortality that
155 simultaneously models two categories of virus ("B.1.617.2" and "non-B.1.617.2") and that
156 allows for epidemiological properties (such as transmissibility and capacity to reinfect
157 previously infected individuals) to vary between categories[16]. Full mathematical details and a
158 simulation study are given in **Supplementary information (**and code is available on GitHub).
159 This model explicitly incorporates waning of immune protection following infection,
160 parameterised using the results of recent longitudinal cohort studies[17,18]. The model integrates
161 epidemiological data on daily COVID-19 mortality (api.covid19india.org), serological data
162 from the city spanning July - December 2020 [18] and genomic sequence data from GISAID (with
163 lineage classification carried out using the Pangolin software tool (https://pangolin.cog-
164 uk.io/)[19] (**Figure 1b,c).** Importantly, the model makes the assumption of a homogeneously
165 mixed population and therefore ignores heterogeneities in contact patterns and degrees of
166 exposures between different sub-groups such as healthcare or service workers where social
167 distancing or working from home is not possible. Such heterogeneities would however likely
168 concentrate new infections in those with a higher chance of having previously being infected,

169 and therefore from this perspective, our estimates of the degree of immune evasion are likely
170 conservative.

171 Given the uncertainties in the date of B.1.617.2 introduction into Mumbai, and the degree of
172 COVID-19 death under-ascertainment, we carried out a range of sensitivity analyses modelling
173 different scenarios for both death underreporting and introduction dates, examining the
174 epidemiological properties inferred for B.1.617.2 under each of these scenarios. Full results for
175 the different scenarios are presented in **Extended Data Table 1**. Across each of these
176 scenarios, our results support B.1.617.2 having altered epidemiological properties compared to
177 SARS-CoV-2 lineages co-circulating in the city, and that the most plausible alteration to its
178 epidemiological properties involves both an increase in transmissibility and some degree of
179 immune-evasion. Results for the scenario assuming 50% death underreporting and an
180 introduction date of 31st Jan 2021 (**Figure 1d**) indicate that B.1.617.2 is 1.1- to 1.4-fold (50%
181 bCI) more transmissible (91% posterior probability that increase is > 1) than co-circulating
182 lineages in Mumbai (predominantly B.1.617.1 and B.1.1.7). These lineages have been
183 estimated to be >1.5 fold more transmissible than non-variant lineages.[1,20]. Furthermore, the
184 results indicate that B.1.617.2 is able to evade 16 to 55% of the immune protection provided
185 by prior infection with non-B.1.617.2 lineages, with a 96% probability that immune evasion is
186 > 5%. [1,20]

187 Important caveats to our Bayesian modelling results include the use of serological data derived
188 from a convenience sample of self-referring individuals presenting for testing, as well as
189 significant uncertainties about the sampling frameworks underlying the SARS-CoV-2
190 genomic sequences available on GISAID. We also highlight that these results may not
191 generalise to other settings. For example, our estimates of immune evasion are made in a
192 setting in which a significant amount of immunity has been derived from previous infection,
193 limiting their generalisability to settings in which vaccine-derived immunity predominates
194 (given evidence suggesting differences in the immune responses elicited by vaccination
195 compared to previous infection[21]).
196

197 **B.1.617.2 shows reduced sensitivity to neutralising antibodies from recovered individuals**
198 We next sought biological support for the inferences from mathematical modelling, starting
199 with immune evasion to antibody responses generated by previous SARS-CoV-2 infection. We
200 used sera from twelve individuals infected during the first UK wave in mid-2020 (likely

201 following infection with SARS-CoV-2 Wuhan-1). These sera were tested for ability to
202 neutralise a B.1.617.2 viral isolate (obtained from nose/throat swab), in comparison to a B.1.1.7
203 variant isolate, a wild type (WT) Wuhan-1 virus bearing D614G in spike, and B.1.351 (Beta)
204 variant. The Delta variant contains several spike mutations that are located at positions within
205 the structure that are predicted to alter its function (**Figure 1e**). We found that the B.1.1.7 virus
206 isolate was 2.3-fold less sensitive to the sera, and that B.1.617.2 was 5.7-fold less sensitive to
207 the sera compared to the WT. Importantly in the same assay, the B.1.351 (Beta) variant that
208 emerged in South Africa demonstrated an 8.2-fold loss of neutralisation sensitivity relative to
209 WT (**Figure 1f**).
210
211 **B.1.617.2 shows reduced sensitivity to vaccine-elicited antibodies**
212 We used a B.1.617.2 live virus isolate to test susceptibility to vaccine elicited serum
213 neutralising antibodies in individuals following vaccination with two doses ChAdOx-1 or
214 BNT162b2. These experiments showed a loss of sensitivity for B.1.617.2 compared to wild
215 type Wuhan-1 bearing D614G of around 8-fold for both sets of vaccine sera and reduction
216 against B.1.1.7 that did not reach statistical significance (**Figure 2a**). We also used a
217 pseudotyped virus (PV) system to test neutralisation potency of a larger panel of 65 vaccine-
218 elicited sera (**Extended Data Table 2**), this time against PV bearing B.1.617.1 as well as
219 B.1.617.2 spike compared to Wuhan-1 D614G spike (**Figure 2b**). Comparison of demographic
220 data for each individual showed similar characteristics (**Extended Data Table 2**). The mean
221 GMT against Delta Variant spike PV was lower for ChAdOx-1 compared to BNT162b2 (GMT
222 3372 versus 654, p<0001, **Extended Data Table 2)**.
223
224 **B.1.617.2 is less sensitive to monoclonal antibodies (mAbs)**
225 We investigated the sensitivity of B.1.617.2 spike to neutralising antibodies by testing 33 (3
226 NTD, 21 RBM- and 9 non-RBM-specific) spike-specific mAbs isolated from 6 individuals that
227 recovered from WT SARS-CoV-2 infection. We performed a neutralization assay using Vero
228 E6 target cells expressing Transmembrane protease serine 2 (TMPRSS2) infected with PV
229 bearing the Wuhan-1 D614G SARS-CoV-2 spike or the B.1.617.2 spike (**Figure 2c**, **Extended**
230 **Data Figure 1a-c and Extended Data Table 3**). In addition, 5 clinical-stage receptor-binding
231 motif (RBM)-mAbs (etesevimab, casirivimab, regdanvimab, imdevimab and bamlanivimab)
232 were also tested (**Figure 2e, Extended Data Figure 1d and Extended Data Table 3**). We
233 found that all three NTD-mAbs (100%) and four out of nine (44%) non-RBM mAbs completely
234 lost neutralizing activity against B.1.617.2 (**Figure 2 d-e and Extended Data Figure 1a**).

235 Within the RBM-binding group, 16 out 25 mAbs (76%) showed a marked decrease (2-35 fold-
236 change reduction) or complete loss (>40 fold-change reduction) of neutralizing activity to
237 B.1.617.2, suggesting that in a sizeable fraction of RBM antibodies the L452R and T478K
238 mutations are responsible for their loss of neutralizing activity (**Figures 2d-e, Extended Data**
239 **Figure 1b**). Amongst the clinical-stage RBM-mAbs tested, bamlanivimab, which showed
240 benefit in a clinical trial against prior variants[22], did not neutralize B.1.617.2. Imdevimab, part
241 of the REGN-COV2 therapeutic dual antibody cocktail[23], as well as regdanvimab, displayed
242 reduced neutralizing activity. The remaining clinical-stage mAbs, including S309 (the parental
243 antibody from which sotrovimab was derived), retained potent neutralizing activity against
244 B.1.617.2.
245
246 **B.1.617.2 variant shows higher replication in human airway model systems**
247 We next sought biological evidence for the higher transmissibility predicted from the
248 modelling. Increased replication could be responsible for generating greater numbers of virus
249 particles, or the particles themselves could be more likely to lead to a productive infection. We
250 first infected a lung epithelial cell line, Calu-3, comparing B.1.1.7 and B.1.617.2 (**Figure 3a-**
251 **d**). We observed a replication advantage for B.1.617.2 as demonstrated by increase in
252 intracellular RNA transcripts and Spike and Nucleocapsid proteins compared to B.1.1.7
253 (**Figure 3a-b)**, as well as an increase in released virions from infected cells (**Figure 3c-d**). Next
254 we tested B.1.1.7 against two separate isolates of B.1.617.2 in a human airway epithelial model
255 [24]. In this system we again observed that both B.1.617.2 isolates had a significant replication
256 advantage over B.1.1.7 (**Figure 3e-f)**. Finally, we infected primary 3D airway organoids[25]
257 (**Figure 3g**) with B.1.617.2 and B.1.1.7 virus isolates, noting a significant replication
258 advantage for B.1.617.2 over B.1.1.7. These data clearly support higher replication rate and
259 therefore transmissibility of B.1.617.2 over B.1.1.7.
260
261 In the aforementioned experiments (**Figure 3b**), we noted a higher proportion of intracellular
262 B.1.617.2 spike in the cleaved state in comparison to B.1.1.7. In order to investigate this further
263 we produced the two viruses as well as a Wuhan-1 WT D614G virus in Vero-hACE2-
264 TMPRSS2 cells, harvested and purified virus from culture supernatants at 48 hours. This
265 analysis showed that the B.1.617.2 spike was predominantly in the cleaved form, in contrast to
266 WT and B.1.1.7 (**Extended Data Figure 3a-b**).
267
268 **B.1.617.2 spike has enhanced entry efficiency associated with cleaved spike**

269 SARS-CoV-2 Spike is known to mediate cell entry via interaction with ACE2 and TMPRSS2[26]
270 and is a major determinant of viral infectivity. In order to gain insight into the mechanism of
271 increased infectivity of B.1.617.2, we tested single round viral entry of B.1.617.1 and B.1.617.2
272 spikes (**Extended Data Figure 2a-b**) using the pseudotyped virus (PV) system, infecting Calu-
273 3 lung cells expressing endogenous levels of ACE2 (Angiotensin Converting Enzyme 2) and
274 TMPRSS2 (Transmembrane protease serine 2) (**Figure 3j**), as well as other cells transduced
275 or transiently transfected with ACE2 / TMPRSS2 (**Extended Data Figure 2b**). We first probed
276 PV virions and cell lysates for spike protein and noted that the B.1.617 spikes were present
277 predominantly in cleaved form in cells and virions, in contrast to WT (**Figure 3h-I, Extended**
278 **Data Figure 2c**). We observed one log increased entry efficiency for both B.1.617.1 and
279 B.1.617.2. over Wuhan-1 D614G wild type in nearly all cells tested (**Extended Data Figure**
280 **2b**). In addition, B.1.617.2 appeared to have an entry advantage compared to B.1.617.1 in some
281 cells, and in particular Calu-3 bearing endogenous receptor levels (**Figure 3j**). Finally, we
282 wished to confirm higher infectivity using live virus isolates of B.1.617.1 and B.1.617.2. As
283 expected from the PV comparison, B.1.617.2 showed increased replication kinetics over
284 B.1.617.1 in Calu-3 cells as measured by viral RNA in cells and $TCID_{50}$ of released virions
285 (**Figure 3k**).
286
287 **B.1.617.2 spike confers increased syncytium formation**
288 The plasma membrane route of entry, and indeed transmissibility in animal models, is critically
289 dependent on the polybasic cleavage site (PBCS) between S1 and S2[24,27,28]and cleavage of
290 spike prior to virion release from producer cells; this contrasts with the endosomal entry route,
291 which does not require spike cleavage in producer cells. [24,29,30]. Mutations at P681 in the PBCS
292 have been observed in multiple SARS-CoV-2 lineages, most notably in the B.1.1.7 Alpha
293 variant[31]. We previously showed that B.1.1.7 spike, bearing P681H, had significantly higher
294 fusogenic potential than a D614G Wuhan-1 virus[29]. Here we tested B.1.617.1 and B.1.617.2
295 spike using a split GFP system to monitor cell-cell fusion (**Figure 4a, b, c**). We transfected
296 spike bearing plasmids into Vero cells stably expressing the two different parts of Split-GFP,
297 so that GFP signal could be measured over time upon cell-cell fusion (**Figure 4d**). The
298 B.1.617.1 and B.1.617.2 spike proteins mediated higher fusion activity and syncytium
299 formation than WT, but were similar to B.1.1.7 (**Figure 4d,e**). The single P681R mutation was
300 able to recapitulated this phenotype (**Figure 4d,e**). We next tested the ability of furin inhibitor
301 CMK[32-34] to inhibit cell-cell fusion, a process that requires cleaved spike. We found that fusion
302 mediated by the B.1.617.2 spike was marginally less sensitive to CMK relative to Wuhan-1

303 WT D614G (Fold change 1.6 [95% CI 1.4-1.8, $p<0.05$], **Figure 4f**). Finally, we explored
304 whether post vaccine sera could block syncytia formation, as this might be a mechanism for
305 vaccine protection against pathogenesis. We titrated sera from ChAdOx-1 vaccinees and
306 showed that indeed the cell-cell fusion could be inhibited in a manner that mirrored
307 neutralisation activity of the sera against PV infection of cells (**Figure 4g**). Hence B.1.617.2
308 may induce cell-cell fusion in the respiratory tract and possibly higher pathogenicity even in
309 vaccinated individuals with neutralising antibodies.
310
311 **Breakthrough B.1.617.2 infections in ChAdOx-1 vaccinated health care workers**
312 Hitherto we have gathered epidemiological and biological evidence that the growth advantage
313 of B.1.617.2 might relate to increased virus replication/transmissibility as well as re-infection
314 due to evasion of neutralising antibodies from prior infection. We hypothesised that clinical
315 vaccine efficacy against B.1.617.2 would be compromised relative to other circulating variants.
316 Although overall national vaccination rates were low in India in the first quarter of 2021,
317 vaccination of health care workers (HCW) started in early 2021 with the ChAdOx-1 vaccine
318 (Covishield). During the wave of infections during March and April, an outbreak of
319 symptomatic SARS-CoV-2 was confirmed in 30 vaccinated staff members amongst an overall
320 workforce of 3800 at a single tertiary centre in Delhi by RT-PCR of nasopharyngeal swabs
321 (age range 27-77 years). Genomic data from India suggested B.1.1.7 dominance overall
322 (**Figure 1a**) and in the Delhi area during the first quarter of 2021 (**Figure 5a**), with growth of
323 B.1.617 during March 2021. By April 2021, 385 out of 604 sequences reported to GISAID for
324 Delhi were B.1.617.2. Short-read sequencing[35] of symptomatic individuals in the HCW
325 outbreak revealed the majority were B.1.617.2 with a range of other B lineage viruses including
326 B.1.1.7 and B.1.617.1 (**Figure 5b**). There were no cases that required ventilation though one
327 HCW received oxygen therapy. Phylogenetic analysis demonstrated a group of highly related,
328 and in some cases, genetically indistinct sequences that were sampled within one or two days
329 of each other (**Figure 5b**). These data are consistent with a single transmission from an infected
330 individual, constituting an over dispersion or 'super spreader' event. We next looked in greater
331 detail at the vaccination history of cases. Nearly all had received two doses at least 21 days
332 previously, and median time since second dose was 27 days (**Figure 5b, Supplementary**
333 **information**).
334
335 We obtained similar data on breakthrough infections and ChAdOx-1 vaccination status in two
336 other health facilities in Delhi with 1100 and 4000 HCW staff members respectively (**Figure**

337 **5c-d**). In hospital two there were 106 sequences from symptomatic infections. After filtering,
338 we reconstructed phylogenies using 66 with high quality whole genome coverage >95%; in
339 hospital three there were 65 symptomatic infections from which genomes were generated, with
340 52 high quality genomes used for inferring phylogenies after filtering (**Figure 5c-d**). As
341 expected from variants circulating in the community, we observed that B.1.617.2 dominated
342 vaccine-breakthrough infections in both centres (**Figure 5c-d, Extended Data Table 4a**). The
343 magnitude of vaccine responses in a small sample of HCW with subsequent breakthrough was
344 measured and appeared similar to responses in a control group of HCW that did not test positive
345 for SARS-CoV-2 subsequently (**Extended Data Figure 3a**). Analysis of Ct values in positive
346 samples did not show significant differences between HCW infected with B.1.617.2 versus
347 non- B.1.617.2 (**Extended Data Figure 3b, Supplementary information**).
348
349 Finally, we evaluated the effect of B.1.617.2 on vaccine efficacy against symptomatic
350 infection in the HCWs. Ideally one would use a randomised controlled trial for such an
351 analysis, though a placebo arm is not ethical at present. In terms of observational studies, one
352 would ideally have used a test negative case control approach. Given the lack of availability
353 of test negative data in our HCW setting we used an alternative approach to estimate VE used
354 by Public Health England (PHE)[36]. If the vaccine had equal efficacy against B.1.617.2 and
355 non-B.1.617.2, a similar proportion of B.1.617.2 and non-B.1.617.2 breakthrough cases
356 would be expected in both vaccinated and unvaccinated individuals. However, in our HCW,
357 non-B.1.617.2 was isolated in a lower proportion of symptomatic cases in the fully
358 vaccinated group compared to unvaccinated cases (**Extended Data Table 4b**). We used
359 multivariable logistic regression to estimate the odds ratio of testing positive with B.1.617.2
360 versus non- B.1.617.2 in vaccinated relative to unvaccinated individuals, adjusting for age,
361 sex and hospital. The adjusted odds ratio for B.1.617.2 relative to non-B.1.617.2 was 5.14
362 (95% CI 1.32-20.0, p=0.018) for two vaccine doses (**Extended Data Table 4b**). This
363 indicates that vaccine efficacy against B.1.617.2 is reduced relative to non- B.1.617.2 viruses
364 that included B.1.1.7, B.1 and B.1.617.1. These data are consistent with those derived in the
365 UK where the non-B.1.617.2 infections were largely B.1.1.7[36].
366
367 **Discussion**
368 Here we have combined mathematical modelling, molecular epidemiology and *in vitro*
369 experimentation to propose that increased replication fitness and reduced sensitivity of
370 B.1.617.2 to neutralising antibodies from past infection contributed to the devastating epidemic

371 wave in India during the first quarter of 2021, where background infection to the Wuhan-1 WT
372 D614G in 2020 was between 20-50%[37] and vaccination with at least one dose below 20%. The
373 proposed contribution of both immune evasion and increased transmissibility would also
374 explain the recent rapid replacement of B.1.1.7 by B.1.617.2 in the UK
375 (https://www.gisaid.org), where vaccination rates are high in adults and infections not confined
376 to the unvaccinated[36].
377
378 We demonstrate evasion of neutralising antibodies by a B.1.617.2 live virus with sera from
379 convalescent patients, as well as sera from individuals vaccinated with two different vaccines,
380 one based on an adenovirus vector (ChAdOx-1), and the other mRNA based (BNT162b2). Our
381 findings on reduced susceptibility of B.1.617.2 to vaccine elicited sera are similar to other
382 reports[38,39], including the lower GMT following two doses of ChAdOx-1 compared to
383 BNT162b2[38]. Although we did not map the mutations responsible, previous work with shows
384 that L452R and T478K in the spike RBD are likely to have contributed[9], as well as spike NTD
385 mutations such as T19R, R158G and the deletion at spike amino acid positions 156 and 157.
386 The importance of NTD in both cell entry efficiency[29,40] as well as antibody evasion is
387 increasingly recognised[41,42] and further work is needed to map specific determinants in the
388 B.1.617.2 NTD.
389
390 We also report ChAdOx-1 vaccine breakthrough infections in health care workers at three
391 Delhi hospitals, most of whom were fully vaccinated. These infections were predominantly
392 B.1.617.2, with a mix of other lineages including B.1.1.7, reflecting prevalence in community
393 infections. We estimated the relative vaccine efficacy of ChAdOx-1 vaccination in our HCW
394 analysis against B.1.617.2 versus other lineages, finding an increased odds of infection with
395 B.1.617.2 compared to non- B.1.617.2 following two doses. These data indicate reduced
396 vaccine efficacy against B.1.617.2 and support an immune evasion advantage for B.1.617.2
397 and are in concordance with *in vitro* data from neutralizing assays. It is important to consider
398 that increased infectivity at mucosal surfaces and cell-cell fusion and spread[43] may also
399 facilitate 'evasion' from antibodies[44]. We showed that B.1.617.2 fused cells efficiently, and
400 that blockade of this process by vaccine-elicited antibodies was compromised for B.1.617.2,
401 potentially allowing it to spread locally in respiratory tissue at higher rate even in the context
402 of vaccination.
403

404 Indeed, our work also shows that that B.1.617.2 had a fitness advantage compared to B.1.1.7
405 across physiologically relevant systems including HAE[45] and 3D airway organoids[25] where
406 cell free and cell-cell infection are likely to be occurring together. These data support the notion
407 of higher infectiousness of B.1.617.2, either due to higher viral burden or higher particle
408 infectivity, resulting in higher probability of person to person transmission. Similarly, we were
409 also able to report that B.1.617.2 has a replication advantage in lung cells compared to
410 B.1.617.1, at least partially driven by spike. Given our data showing that B.1.617.2 and
411 B.1.617.1 spikes confer similar sensitivities to sera from vaccinees, increased fitness is a
412 parsimonious explanation for the growth advantage of B.1.617.2 over B.1.617.1.
413
414 Virus infectivity and fusogenicity mediated by the PBCS is a key determinant of pathogenicity
415 and transmissibility[24,46] and there are indications that giant cells/syncytia formation are
416 associated with fatal disease[47]. Spike cleavage and stability of cleaved spike are likely therefore
417 to be critical parameters for future SARS-CoV-2 variants of concern. B.1.617.2 had similar
418 kinetics of syncytia formation as compared to B.1.1.7, likely attributable to P681R. We show
419 that vaccine-elicited sera can inhibit syncytia, and that this is compromised for B.1.617.2.
420
421 Compromise of bamlanivimab, but not imedevimab, was previously noted for B.1.617.1 and
422 B.1.617.2[4,48]. The REGN-COV2 dual monoclonal antibody therapy containing casirivimab and
423 imedevimab was shown to improve survival[49], and our data showing reduced efficacy for
424 imedevimab against B.1.617.2 might compromise clinical efficacy. Moreover, it could lead to
425 possible selection of escape variants where there is immune compromise and chronic SARS-
426 CoV-2 infection with B.1.617.2[50]. Further work to explore these possibilities is urgently
427 needed.
428
429 Although weaker protection against infection with B.1.351 (Beta) (the variant with least
430 sensitivity to neutralising antibodies) has been demonstrated for at least three vaccines[12,51-53],
431 progression to severe disease and death has been low. Therefore, at population scale, extensive
432 vaccination will likely protect against moderate to severe disease due to B.1.617.2. Indeed,
433 data from the UK already demonstrate low incidence of severe disease in vaccinees (PHE
434 technical report 17). However, our data on ChAdOx-1 vaccine breakthrough and reduced
435 vaccine efficacy against symptomatic B.1.617.2 infection are of concern given that hospitals
436 frequently treat individuals who may have suboptimal immune responses to vaccination due to
437 comorbidity. Such patients could be at risk for severe disease following infection from HCW

438 or other staff within hospital environments. Transmissions in vaccinated HCW could
439 potentially involve overdispersion or 'super-spreading'[54], and indeed we document such an
440 event in one of three hospitals studied. Therefore strategies to boost vaccine responses against
441 variants are warranted in HCW and attention to infection control procedures should be
442 continued even in the post vaccine era.
443
444
445
446
447
448
449 **Methods**
450 *Sequencing Quality Control and Phylogenetic Analysis*
451 Three sets of fasta concensus sequences were kindly provided by three separate Hospitals in
452 Delhi, India. Initially, all sequences were concatenated into a multi-fasta, according to hospital,
453 and then aligned to reference strain MN908947.3 (Wuhan-Hu-1) with mafft v4.475 [55] using
454 the --keeplength --addfragments options. Following this, all sequences were passed through
455 Nextclade v0.15 (https://clades.nextstrain.org/) to determine the number of gap regions. This
456 was noted and all sequences were assigned a lineage with Pangolin v3.1.5[19] and pangoLEARN
457 (dated 15th June 2021). Sequences that could not be assigned a lineage were discarded. After
458 assigning lineages, all sequences with more than 5% N-regions were also excluded.
459
460 Phylogenies were inferred using maximum-likelihood in IQTREE v2.1.4[56] using a GTR+R6
461 model with 1000 rapid bootstraps. The inferred phylogenies were annotated in R v4.1.0 using
462 ggtree v3.0.2[57] and rooted on the SARS-CoV-2 reference sequence (MN908947.3). Nodes
463 were arranged in descending order and lineages were annotated on the phylogeny as coloured
464 tips, alongside a heatmap defining the number of ChAdOx-1 vaccines received from each
465 patient.
466
467 *Area plots and metadata*
468 Area plots were constructed in RStudio v4.1.0 using the ggplot2 package v3.3.3. Data to
469 populate the plot was downloaded from the GISAID[58] (http://gisaid.org) database. Sequence
470 metadata for the entire database was downloaded on 8th June 2021 and filtered by location

471 (United Kingdom, or Asia / India). The number of assigned lineages was counted for each
472 location and the most prevalent 15 lineages were retained for plotting.
473
474 *Structural Analyses*
475 The PyMOL Molecular Graphics System v.2.4.0 (https://github.com/schrodinger/pymol-open-
476 source/releases) was used to map the location of the mutations defining the Delta lineage
477 (B.1.617.2) onto closed-conformation spike protein - PDB: 6ZGE[59].
478
479 *Statistical Analyses*
480 Descriptive analyses of demographic and clinical data are presented as median and interquartile
481 range (IQR) or mean and standard deviation (SD) when continuous and as frequency and
482 proportion (%) when categorical. The difference in continuous and categorical data were tested
483 using Wilcoxon rank sum or T-test and Chi-square test respectively. Linear regression was
484 used to model the association between transmission chain size and lineage. The effect of
485 clustering by hospital was taken into account in the regression analysis. All non-B.1.617.2
486 lineages were grouped into one category. The neutralisation by vaccine-elicited antibodies after
487 the two doses of the BNT162b2 and Chad-Ox-1 vaccine was determined. The ID50 within
488 groups were summarised as a geometric mean titre (GMT) and statistical comparison between
489 groups were made with Mann-Whitney or Wilcoxon ranked sign test. Statistical analyses were
490 done using Stata v13 and Prism v9.
491
492 *Serum samples and ethical approval*
493 Ethical approval for use of serum samples. Controls with COVID-19 were enrolled to the
494 NIHR BioResource Centre Cambridge under ethics review board (17/EE/0025).
495
496 *Pseudotype virus experiments*
497 *Cells*
498 HEK 293T CRL-3216, Hela-ACE-2 (Gift from James Voss), Vero CCL-81 were maintained
499 in Dulbecco's Modified Eagle Medium (DMEM) supplemented with 10% fetal calf serum
500 (FCS), 100 U/ml penicillin, and 100mg/ml streptomycin. All cells were regularly tested and
501 are mycoplasma free. H1299 cells were a kind gift from Sam Cook. Calu-3 cells were a kind
502 gift from Paul Lehner, A549 A2T2[60] cells were a kind gift from Massimo Palmerini. Vero E6
503 Ace2/TMPRSS2 cells were a kind gift from Emma Thomson.
504

505 *Pseudotype virus preparation for testing against vaccine elicited antibodies and cell entry*
506 Plasmids encoding the spike protein of SARS-CoV-2 D614 with a C terminal 19 amino acid
507 deletion with D614G were used. Mutations were introduced using Quickchange Lightning Site-
508 Directed Mutagenesis kit (Agilent) following the manufacturer's instructions. B.1.1.7 S
509 expressing plasmid preparation was described previously, but in brief was generated by step
510 wise mutagenesis. Viral vectors were prepared by transfection of 293T cells by using Fugene
511 HD transfection reagent (Promega). 293T cells were transfected with a mixture of 11ul of
512 Fugene HD, 1µg of pCDNAΔ19 spike-HA, 1ug of p8.91 HIV-1 gag-pol expression vector and
513 1.5µg of pCSFLW (expressing the firefly luciferase reporter gene with the HIV-1 packaging
514 signal). Viral supernatant was collected at 48 and 72h after transfection, filtered through
515 0.45um filter and stored at -80˚C as previously described. Infectivity was measured by
516 luciferase detection in target 293T cells transfected with TMPRSS2 and ACE2.
517
518 *Standardisation of virus input by SYBR Green-based product-enhanced PCR assay (SG-PERT)*
519 The reverse transcriptase activity of virus preparations was determined by qPCR using a SYBR
520 Green-based product-enhanced PCR assay (SG-PERT) as previously described[61]. Briefly, 10-
521 fold dilutions of virus supernatant were lysed in a 1:1 ratio in a 2x lysis solution (made up of
522 40% glycerol v/v 0.25% Triton X-100 v/v 100mM KCl, RNase inhibitor 0.8 U/ml, TrisHCL
523 100mM, buffered to pH7.4) for 10 minutes at room temperature.
524
525 12µl of each sample lysate was added to thirteen 13µl of a SYBR Green master mix (containing
526 0.5µM of MS2-RNA Fwd and Rev primers, 3.5pmol/ml of MS2-RNA, and 0.125U/µl of
527 Ribolock RNAse inhibitor and cycled in a QuantStudio. Relative amounts of reverse
528 transcriptase activity were determined as the rate of transcription of bacteriophage MS2 RNA,
529 with absolute RT activity calculated by comparing the relative amounts of RT to an RT
530 standard of known activity.
531
532 *Viral isolate comparison between B.1.617.1 and B.1.617.2*
533 *Cell Culture*
534 VeroE6/TMPRSS2 cells [an African green monkey (*Chlorocebus sabaeus*) kidney cell line;
535 JCRB1819][62] were maintained in Dulbecco's modified Eagle's medium (low glucose) (Wako,
536 Cat# 041-29775) containing 10% FCS, G418 (1 mg/ml; Nacalai Tesque, Cat# G8168-10ML)
537 and 1% antibiotics (penicillin and streptomycin; PS).

538 Calu-3 cells (a human lung epithelial cell line; ATCC HTB-55) were maintained in Minimum
539 essential medium Eagle (Sigma-Aldrich, Cat# M4655-500ML) containing 10% FCS and 1%
540 PS.
541
542 *SARS-CoV-2 B.1.617.1 vs B.1.617.2 Preparation, Titration and infection of Calu-3*
543 Two viral isolates belonging to the B.1.617 lineage, B.1.617.1 (GISAID ID:
544 EPI_ISL_2378733) and B.1.617.2 (GISAID ID: EPI_ISL_2378732) were isolated from
545 SARS-CoV-2-positive individuals in Japan. Briefly, 100 µl of the nasopharyngeal swab
546 obtained from SARS-CoV-2-positive individuals were inoculated into VeroE6/TMPRSS2
547 cells in the biosafety level 3 laboratory. After the incubation at 37°C for 15 minutes, a
548 maintenance medium supplemented [Eagle's minimum essential medium (FUJIFILM Wako
549 Pure Chemical Corporation, Cat# 056-08385) including 2% FCS and 1% PS] was added, and
550 the cells were cultured at 37°C under 5% CO_2. The cytopathic effect (CPE) was confirmed
551 under an inverted microscope (Nikon), and the viral load of the culture supernatant in which
552 CPE was observed was confirmed by real-time RT-PCR. To determine viral genome
553 sequences, RNA was extracted from the culture supernatant using QIAamp viral RNA mini kit
554 (Qiagen, Qiagen, Cat# 52906). cDNA library was prepared by using NEB Next Ultra RNA
555 Library Prep Kit for Illumina (New England Biolab, Cat# E7530) and whole genome
556 sequencing was performed by Miseq (Illumina).
557
558 To prepare the working virus, 100 µl of the seed virus was inoculated into VeroE6/TMPRSS2
559 cells (5,000,000 cells in a T-75 flask). At one hour after infection, the culture medium was
560 replaced with Dulbecco's modified Eagle's medium (low glucose) (Wako, Cat# 041-29775)
561 containing 2% FBS and 1% PS; at 2-3 days postinfection, the culture medium was harvested
562 and centrifuged, and the supernatants were collected as the working virus.
563
564 The titer of the prepared working virus was measured as 50% tissue culture infectious dose
565 ($TCID_{50}$). Briefly, one day prior to infection, VeroE6/TMPRSS2 cells (10,000 cells/well) were
566 seeded into a 96-well plate. Serially diluted virus stocks were inoculated to the cells and
567 incubated at 37°C for 3 days. The cells were observed under microscopy to judge the CPE
568 appearance. The value of $TCID_{50}$/ml was calculated with the Reed-Muench method[63].
569
570 One day prior to infection, 20, 000 Calu-3 cells were seeded into a 96-well plate. SARS-CoV-
571 2 (200 $TCID_{50}$) was inoculated and incubated at 37°C for 1 h. The infected cells were washed,

572 and 180 µl of culture medium was added. The culture supernatant (10 µl) was harvested at
573 indicated time points and used for real-time RT-PCR to quantify the viral RNA copy number.
574
575 *Real-Time RT-PCR*
576 Real-time RT-PCR was performed as previously described[64,65]. Briefly, 5 µl of culture
577 supernatant was mixed with 5 µl of 2 × RNA lysis buffer [2% Triton X-100, 50 mM KCl, 100
578 mM Tris-HCl (pH 7.4), 40% glycerol, 0.8 U/µl recombinant RNase inhibitor (Takara, Cat#
579 2313B)] and incubated at room temperature for 10 min. RNase-free water (90 µl) was added,
580 and the diluted sample (2.5 µl) was used as the template for real-time RT-PCR performed
581 according to the manufacturer's protocol using the One Step TB Green PrimeScript PLUS RT-
582 PCR kit (Takara, Cat# RR096A) and the following primers: Forward *N*, 5'-AGC CTC TTC
583 TCG TTC CTC ATC AC-3'; and Reverse *N*, 5'-CCG CCA TTG CCA GCC ATT C-3'. The
584 copy number of viral RNA was standardized with a SARS-CoV-2 direct detection RT-qPCR
585 kit (Takara, Cat# RC300A). The fluorescent signal was acquired using a QuantStudio 3 Real-
586 Time PCR system (Thermo Fisher Scientific), a CFX Connect Real-Time PCR Detection
587 system (Bio-Rad) or a 7500 Real Time PCR System (Applied Biosystems).
588
589 *Virus growth kinetics in HAE cells*
590 Primary nasal human airway epithelial (HAE) cells at air-liquid interface (ALI) were purchased
591 from Epithelix and the basal MucilAir medium (Epithelix) was changed every 2-3 days for
592 maintenance of HAE cells. All dilution of viruses, wash steps and harvests were carried out
593 with OptiPRO SFM (Life Technologies) containing 2X GlutaMAX (Gibco). All wash and
594 harvest steps were performed by addition of 200ul SFM to the apical surface and incubation
595 for 10 mins at 37°C before removing SFM. To infect, basal medium was replaced, the apical
596 surface of the HAE cells washed once with SFM to remove mucus before addition of virus to
597 triplicate wells. Cells were infected at a multiplicity of 1e4 genomes copies of virus per cell
598 based on E gene qRT-PCR. Inoculum was incubated for 1 h at 37°C before removing, washing
599 the apical surface twice and the second wash taken as harvest for 0 hpi. A single apical wash
600 was performed to harvest virus at 24, 48 and 71 hr timepoints. Isolates used were B.1.617.2
601 isolate #60 hCoV-19/England/SHEF-10E8F3B/2021 (EPI_ISL_1731019), B.1.617.2 isolate
602 #285 hCoV-19/England/PHEC-3098A2/2021 (EPI_ISL_2741645) and B.1.1.7 isolate #7540
603 SMH2008017540 (confirmed B.1.1.7 in-house but not yet available on GISAID).
604

Subtype	Name	Sequencing	19	77	142	156-158	222	452	478	614	681	950
Wuhan	Wuhan	-	T	K	G	WT	A	L	T	D	P	D
B.1.617.2	**60**	VAT2	R	R	D	del	V	R	K	G	R	N
B.1.617.2	**285**	VAT2	R		D	del	V	R	K	G	R	N

605
606
607
608 *Titration of outputs from HAE infections*
609 For determining genome copies in the virus inputs and in the supernatant harvested from HAE
610 cells, RNA was extracted using QIAsymphony DSP Virus/Pathogen Mini Kit on the
611 QIAsymphony instrument (Qiagen). qRT-PCR was then performed using AgPath RT-PCR
612 (Life Technologies) kit on a QuantStudio(TM) 7 Flex System with the primers for SARS-CoV-
613 2 E gene used in Corman et al., (2020). A standard curve was also generated using dilutions
614 viral RNA of known copy number to allow quantification of E gene copies in the samples from
615 Ct values. E gene copies per ml of original virus supernatant were then calculated.
616
617 For measuring infectious virus in harvests from HAE cells, plaque assays were performed by
618 performing serial log dilutions of supernatant in DMEM, 1% NEAA and 1% P/S and
619 inoculating onto PBS-washed Vero cells, incubating for 1 hr at 37°C, removing inoculum and
620 overlaying with 1× MEM, 0.2% w/v BSA, 0.16% w/v NaHCO3, 10 mM HEPES, 2mM L-
621 Glutamine, 1× P/S, 0.6% w/v agarose. Plates were incubated for 3 d at 37 °C before overlay
622 was removed and cells were stained for 1 h at room temperature in crystal violet solution.
623
624 *Lung organoid infection by replication competent SARS-CoV-2 isolates.*
625 Airway epithelial organoids were prepared as previously reported. [25] For viral infection
626 primary organoids were passaged and incubated with SARS-CoV-2 in suspension at a
627 multiplicity of infection (MOI) of 1 for 2 hours. Subsequently, the infected organoids were
628 washed twice with PBS to remove the viral particles. Washed organoids were plated in 20 µl
629 Matrigel domes, cultured in organoid medium and harvested at different timepoints.
630 Cells were lysed 24 and 48h post-infection and total RNA isolated. cDNA was synthesized and
631 qPCR was used to determine copies of nucleoprotein gene in samples. Standard curve was
632 prepared using SARS-CoV-2 Positive Control plasmid containing full nucleocapsid protein (N
633 gene) (NEB) and used to quantify copies of N gene in organoid samples. 18S ribosomal RNA
634 was used as a housekeeping gene to normalize sample-to-sample variation.
635

636

637 *Western blotting*

638 Cells were lysed and supernatants collected 18 hours post transfection. Purified virions were
639 prepared by harvesting supernatants and passing through a 0.45 µm filter. Clarified
640 supernatants were then loaded onto a thin layer of 8.4% optiprep density gradient medium
641 (Sigma-Aldrich) and placed in a TLA55 rotor (Beckman Coulter) for ultracentrifugation for 2
642 hours at 20,000 rpm. The pellet was then resuspended for western blotting. Cells were lysed
643 with cell lysis buffer (Cell signalling), treated with Benzonase Nuclease (70664 Millipore) and
644 boiled for 5 min. Samples were then run on 4%–12% Bis Tris gels and transferred onto
645 nitrocellulose or PVDF membranes using an iBlot or semidry (Life Technologies and Biorad,
646 respectively).

647

648 Membranes were blocked for 1 hour in 5% non-fat milk in PBS + 0.1% Tween-20 (PBST) at
649 room temperature with agitation, incubated in primary antibody (anti-SARS-CoV-2 Spike,
650 which detects the S2 subunit of SARS-CoV-2 S (Invitrogen, PA1-41165), anti-GAPDH
651 (proteintech) or anti-p24 (NIBSC)) diluted in 5% non-fat milk in PBST for 2 hours at 4°C with
652 agitation, washed four times in PBST for 5 minutes at room temperature with agitation and
653 incubated in secondary antibodies anti-rabbit HRP (1:10000, Invitrogen 31462), anti-bactin
654 HRP (1:5000; sc-47778) diluted in 5% non-fat milk in PBST for 1 hour with agitation at room
655 temperature. Membranes were washed four times in PBST for 5 minutes at room temperature
656 and imaged directly using a ChemiDoc MP imaging system (Bio-Rad).

657

658 *Virus infection for virion western blotting*

659 Vero-hACE2-TMPRS22 cells were infected with MOI of 1 and incubated for 48
660 hours. Supernatant was cleared by 5 min spin at 300xg and then precipitated with 10%
661 PEG6000 (4h at RT). Pellets were resuspended directly in Laemmli buffer with 1mM
662 DTT, then treated with Benzonase Nuclease(70664 Millipore) and sonicated prior loading for
663 gel electrophoresis

664

665 *Serum pseudotype neutralisation assay*

666 Spike pseudotype assays have been shown to have similar characteristics as neutralisation
667 testing using fully infectious wild type SARS-CoV-2[66].Virus neutralisation assays were
668 performed on 293T cell transiently transfected with ACE2 and TMPRSS2 using SARS-CoV-
669 2 spike pseudotyped virus expressing luciferase[67]. Pseudotyped virus was incubated with serial

670 dilution of heat inactivated human serum samples or convalescent plasma in duplicate for 1h
671 at 37˚C. Virus and cell only controls were also included. Then, freshly trypsinized 293T
672 ACE2/TMPRSS2 expressing cells were added to each well. Following 48h incubation in a 5%
673 CO_2 environment at 37°C, the luminescence was measured using Steady-Glo Luciferase assay
674 system (Promega).
675
676 *Neutralization Assays for convalescent plasma*
677 Convalescent sera from healthcare workers at St. Mary's Hospital at least 21 days since PCR-
678 confirmed SARS-CoV-2 infection were collected in May 2020 as part of the REACT2 study
679 with ethical approval from South Central Berkshire B Research Ethics Committee (REC ref:
680 20/SC/0206; IRAS 283805).
681
682 Convalescent human serum samples were inactivated at 56°C for 30 min and replicate serial 2-
683 fold dilutions (n=12) were mixed with an equal volume of SARs-CoV-2 (100 TCID50; total
684 volume 100 µL) at 37°C for 1 h. Vero-hACE2 TMPRSS2 cells were subsequently infected
685 with serial-fold dilutions of each sample for 3 days at 37°C. Virus neutralisation was quantified
686 via crystal violet staining and scoring for cytopathic effect (CPE). Each-run included 1/5
687 dilutions of each test sample in the absence of virus to ensure virus-induced CPE in each
688 titration. Back-titrations of SARs-CoV-2 infectivity were performed to demonstrate infection
689 with ~100 TCID50 in each well.

690 *Vaccinee Serum neutralization, live virus assays*

691 Vero-Ace2-TMPRSS2 cells were seeded at a cell density of 2x10e4/well in 96w plate 24h
692 before infection. Serum was titrated starting at a final 1:10 dilution with WT (SARS-CoV-
693 2/human/Liverpool/REMRQ0001/2020), B.1.1.7 or B.1.617.2 virus isolates being added at
694 MOI 0.01. The mixture was incubated 1h prior adding to cells. The plates were fixed with 8%
695 PFA 72h post-infection and stained with Coomassie blue for 20 minutes. The plates were
696 washed in water and dried for 2h. 1% SDS was added to wells and staining intensity was
697 measured using FLUOstar Omega (BMG Labtech). Percentage cell survival was determined
698 by comparing intensity of staining to an uninfected wells. A non-linear sigmoidal 4PL model
699 (Graphpad Prism 9.1.2) was used to determine the ID50 for each serum.

700

701 *VSV pseudovirus generation for monoclonal antibody assays*

702 Replication defective VSV pseudovirus expressing SARS-CoV-2 spike proteins corresponding
703 to the different VOC were generated as previously described with some modifications[68]. Lenti-
704 X 293T cells (Takara, 632180) were seeded in 10-cm^2 dishes at a density of 5e6 cells per dish
705 and the following day transfected with 10 µg of WT or B.1.617.2 spike expression plasmid
706 with TransIT-Lenti (Mirus, 6600) according to the manufacturer's instructions. One day post-
707 transfection, cells were infected with VSV-luc (VSV-G) with an MOI of 3 for 1 h, rinsed three
708 times with PBS containing Ca2+/Mg2+, then incubated for an additional 24 h in complete
709 media at 37°C. The cell supernatant was clarified by centrifugation, filtered (0.45 um),
710 aliquoted, and frozen at -80°C.

711

712 *Pseudotyped virus neutralization assay for mAb*

713 Vero E6 expressing TMPRSS2 or not were grown in DMEM supplemented with 10% FBS and
714 seeded into white 96 well plates (PerkinElmer, 6005688) at a density of 20 thousand cells per
715 well. The next day, mAbs were serially diluted in pre-warmed complete media, mixed with
716 WT or B.1.617.2 pseudoviruses and incubated for 1 h at 37°C in round bottom polypropylene
717 plates. Media from cells was aspirated and 50 µl of virus-mAb complexes were added to cells
718 and then incubated for 1 h at 37°C. An additional 100 µL of pre-warmed complete media was
719 then added on top of complexes and cells incubated for an additional 16-24 h. Conditions were
720 tested in duplicate wells on each plate and at least six wells per plate contained untreated
721 infected cells (defining the 0% of neutralization, "MAX RLU" value) and infected cells in the
722 presence of S2E12 and S2X259 at 25 µg/ml each (defining the 100% of neutralization, "MIN
723 RLU" value). Virus-mAb -containing media was then aspirated from cells and 50 µL of a 1:2
724 dilution of SteadyLite Plus (Perkin Elmer, 6066759) in PBS with Ca^{++} and Mg^{++} was added to
725 cells. Plates were incubated for 15 min at room temperature and then were analysed on the
726 Synergy-H1 (Biotek). Average of Relative light units (RLUs) of untreated infected wells
727 (MAX RLU_{ave}) was subtracted by the average of MIN RLU (MIN RLU_{ave}) and used to
728 normalize percentage of neutralization of individual RLU values of experimental data
729 according to the following formula: $(1-(RLU_x - MIN\ RLU_{ave}) / (MAX\ RLU_{ave} - MIN\ RLU_{ave}))$
730 x 100. Data were analyzed and visualized with Prism (Version 9.1.0). IC50 values were
731 calculated from the interpolated value from the log(inhibitor) versus response, using variable
732 slope (four parameters) nonlinear regression with an upper constraint of ≤100, and a lower
733 constrain equal to 0. Each neutralization assay was conducted on two independent experiments,
734 i.e., biological replicates, where each biological replicate contains a technical duplicate. IC50

735 values across biological replicates are presented as arithmetic mean ± standard deviation. The
736 loss or gain of neutralization potency across spike variants was calculated by dividing the
737 variant IC50 by the WT IC50 within each biological replicate, and then visualized as arithmetic
738 mean ± standard deviation.
739
740 *Plasmids for split GFP system to measure cell-cell fusion*
741 pQCXIP-BSR-GFP11 and pQCXIP-GFP1-10 were from Yutaka Hata [69] Addgene plasmid
742 #68716; http://n2t.net/addgene:68716; RRID:Addgene_68716 and Addgene plasmid #68715;
743 http://n2t.net/addgene:68715; RRID:Addgene_68715)
744
745 *Generation of GFP1-10 or GFP11 lentiviral particles*
746 Lentiviral particles were generated by co-transfection of Vero cells with pQCXIP-BSR-GFP11
747 or pQCXIP-GFP1-10 as previously described [70]. Supernatant containing virus particles was
748 harvested after 48 and 72 hours, 0.45 µm filtered, and used to infect 293T or Vero cells to
749 generate stable cell lines. 293T and Vero cells were transduced to stably express GFP1-10 or
750 GFP11 respectively and were selected with 2 µg/ml puromycin.
751
752 *Cell-cell fusion assay*
753 Cell-cell fusion assay was carried out as previously described [70,71] but using a Split-GFP
754 system. Briefly, Vero GFP1-10 and Vero-GFP11 cells were seeded at 80% confluence in a 1:1
755 ration in 24 multiwell plate the day before. Cells. were co-transfected with 0.5 µg of spike
756 expression plasmids in pCDNA3 using Fugene 6 and following the manufacturer's instructions
757 (Promega). Cell-cell fusion was measured using an Incucyte and determined as the proportion
758 of green area to total phase area. Data were then analysed using Incucyte software analysis.
759 Graphs were generated using Prism 8 software. Furin inhibitor CMK (Calbiochem) was added
760 at transfection.
761
762 **Data availability**
763 All fasta consensus sequences files used in this analysis are available from https://gisaid.org or
764 from https://github.com/Steven-Kemp/hospital_india/tree/main/consensus_fasta.
765 Code for the Bayesian modelling analysis is available at:
766 https://github.com/ImperialCollegeLondon/delta_modelling
767
768 **Author contributions**

Conceived study: AA, PR, SAK, DC, SB, SF, SM, RKG, DAC, LP, JB, DP, DC. Designed study and experiments: BM, PM, RKG, JB, NG, LCJ, GP, KS, IATM. Performed experiments: BM, PM, DAC, RD, IATMF, CS-F, CS, JB, LCG, JB, JZ, NG, GBM. Interpreted data: RKG, SAK, AA, SS, JB, RP, PC, PD, KP, VSR, SS, DC, TP, OC, KS, GP, LCJ, WB, SF, SB, DAC, BM, PM, RD, IATMF, PR, JB, KGCS, SM, CW, TM, SB, LP, DC, CS, CS-F and S.F.

Acknowledgments

We would like to thank the Department of Biotechnology, NCDC, RKG is supported by a Wellcome Trust Senior Fellowship in Clinical Science (WT108082AIA). COG-UK is supported by funding from the Medical Research Council (MRC) part of UK Research & Innovation (UKRI), the National Institute of Health Research (NIHR) and Genome Research Limited, operating as the Wellcome Sanger Institute. This study was supported by the Cambridge NIHRB Biomedical Research Centre. We would like to thank Thushan de Silva for the Delta isolate and Kimia Kimelian. SAK is supported by the Bill and Melinda Gates Foundation via PANGEA grant: OPP1175094. I.A.T.M.F. is funded by a SANTHE award (DEL-15-006). We would like to thank Paul Lehner for Calu-3 cells. We would like to thank Clare Lloyd and Sejal Saglani for providing the primary airway epithelial cultures, and James Voss for HeLa ACE2. We thank the Geno2pheno UK consortium. The authors acknowledge support from the G2P-UK National Virology consortium funded by MRC/UKRI (grant ref: MR/W005611/1).This study was also supported by The Rosetrees Trust and the Geno2pheno UK consortium. SF acknowledges the EPSRC (EP/V002910/1). KS is supported by AMED Research Program on Emerging and Re-emerging Infectious Diseases (20fk0108270 and 20fk0108413), JST SICORP (JPMJSC20U1 and JPMJSC21U5) and JST CREST (JPMJCR20H4).

Competing Interests

J.B., C.S.-F., C.S., D.P., D.C. and L.P. are employees of Vir Biotechnology and may hold shares in Vir Biotechnology. RKG has received consulting fees from Johnson and Johnson and GSK.

References

1 Volz, E. *et al.* Assessing transmissibility of SARS-CoV-2 lineage B.1.1.7 in England. *Nature*, doi:10.1038/s41586-021-03470-x (2021).

2 Collier, D. A. *et al.* SARS-CoV-2 B.1.1.7 sensitivity to mRNA vaccine-elicited, convalescent and monoclonal antibodies. *Nature* **593**, 136-141, doi:10.1101/2021.01.19.21249840 (2021).

3 Cherian, S. *et al.* Convergent evolution of SARS-CoV-2 spike mutations, L452R, E484Q and P681R, in the second wave of COVID-19 in Maharashtra, India. *bioRxiv*, 2021.2004.2022.440932, doi:10.1101/2021.04.22.440932 (2021).
4 Hoffmann, M. *et al.* SARS-CoV-2 variant B.1.617 is resistant to Bamlanivimab and evades antibodies induced by infection and vaccination. *bioRxiv*, 2021.2005.2004.442663, doi:10.1101/2021.05.04.442663 (2021).
5 Ferreira, I. *et al.* SARS-CoV-2 B.1.617 emergence and sensitivity to vaccine-elicited antibodies. *bioRxiv*, 2021.2005.2008.443253, doi:10.1101/2021.05.08.443253 (2021).
6 Yadav, P. D. *et al.* Neutralization of variant under investigation B.1.617 with sera of BBV152 vaccinees. *bioRxiv*, 2021.2004.2023.441101, doi:10.1101/2021.04.23.441101 (2021).
7 Deng, X. *et al.* Transmission, infectivity, and antibody neutralization of an emerging SARS-CoV-2 variant in California carrying a L452R spike protein mutation. *medRxiv*, doi:10.1101/2021.03.07.21252647 (2021).
8 McCallum, M. *et al.* SARS-CoV-2 immune evasion by variant B.1.427/B.1.429. *bioRxiv*, 2021.2003.2031.437925, doi:10.1101/2021.03.31.437925 (2021).
9 Motozono, C. *et al.* An emerging SARS-CoV-2 mutant evading cellular immunity and increasing viral infectivity. *bioRxiv*, 2021.2004.2002.438288, doi:10.1101/2021.04.02.438288 (2021).
10 Hadfield, J. *et al.* Nextstrain: real-time tracking of pathogen evolution. *Bioinformatics* **34**, 4121-4123, doi:10.1093/bioinformatics/bty407 (2018).
11 JHU. *CORONA VIRUS RESOURCE CENTRE*, <https://coronavirus.jhu.edu/map.html> (2021).
12 Madhi, S. A. *et al.* Efficacy of the ChAdOx1 nCoV-19 Covid-19 Vaccine against the B.1.351 Variant. *N Engl J Med*, doi:10.1056/NEJMoa2102214 (2021).
13 Kustin, T. *et al.* Evidence for increased breakthrough rates of SARS-CoV-2 variants of concern in BNT162b2 mRNA vaccinated individuals. *medRxiv*, 2021.2004.2006.21254882, doi:10.1101/2021.04.06.21254882 (2021).
14 Collier, D. A. *et al.* Age-related immune response heterogeneity to SARS-CoV-2 vaccine BNT162b2. *Nature*, doi:10.1038/s41586-021-03739-1 (2021).
15 Van Oekelen, O. *et al.* Highly variable SARS-CoV-2 spike antibody responses to two doses of COVID-19 RNA vaccination in patients with multiple myeloma. *Cancer Cell*, doi:10.1016/j.ccell.2021.06.014 (2021).
16 Faria, N. R. *et al.* Genomics and epidemiology of the P.1 SARS-CoV-2 lineage in Manaus, Brazil. *Science*, eabh2644, doi:10.1126/science.abh2644 (2021).
17 Hall, V. J. *et al.* COVID-19 vaccine coverage in health-care workers in England and effectiveness of BNT162b2 mRNA vaccine against infection (SIREN): a prospective, multicentre, cohort study. *Lancet* **397**, 1725-1735, doi:10.1016/S0140-6736(21)00790-X (2021).
18 Velumani, A. *et al.* SARS-CoV-2 Seroprevalence in 12 Cities of India from July-December 2020. *medRxiv*, 2021.2003.2019.21253429, doi:10.1101/2021.03.19.21253429 (2021).
19 Rambaut, A. *et al.* A dynamic nomenclature proposal for SARS-CoV-2 lineages to assist genomic epidemiology. *Nat Microbiol* **5**, 1403-1407, doi:10.1038/s41564-020-0770-5 (2020).
20 Campbell, F. *et al.* Increased transmissibility and global spread of SARS-CoV-2 variants of concern as at June 2021. *Euro Surveill* **26**, doi:10.2807/1560-7917.ES.2021.26.24.2100509 (2021).
21 Greaney, A. J. *et al.* Antibodies elicited by mRNA-1273 vaccination bind more broadly to the receptor binding domain than do those from SARS-CoV-2 infection. *Sci Transl Med* **13**, doi:10.1126/scitranslmed.abi9915 (2021).
22 Chen, P. *et al.* SARS-CoV-2 Neutralizing Antibody LY-CoV555 in Outpatients with Covid-19. *New England Journal of Medicine* **384**, 229-237, doi:10.1056/NEJMoa2029849 (2020).

23 Weinreich, D. M. *et al.* REGN-COV2, a Neutralizing Antibody Cocktail, in Outpatients with Covid-19. *New England Journal of Medicine* **384**, 238-251, doi:10.1056/NEJMoa2035002 (2020).
24 Peacock, T. P. *et al.* The furin cleavage site in the SARS-CoV-2 spike protein is required for transmission in ferrets. *Nat Microbiol*, doi:10.1038/s41564-021-00908-w (2021).
25 Youk, J. *et al.* Three-Dimensional Human Alveolar Stem Cell Culture Models Reveal Infection Response to SARS-CoV-2. *Cell Stem Cell* **27**, 905-919 e910, doi:10.1016/j.stem.2020.10.004 (2020).
26 Hoffmann, M. *et al.* SARS-CoV-2 Cell Entry Depends on ACE2 and TMPRSS2 and Is Blocked by a Clinically Proven Protease Inhibitor. *Cell* **181**, 271-280 e278, doi:10.1016/j.cell.2020.02.052 (2020).
27 Papa, G. *et al.* Furin cleavage of SARS-CoV-2 Spike promotes but is not essential for infection and cell-cell fusion. *PLoS pathogens* **17**, e1009246, doi:10.1371/journal.ppat.1009246 (2021).
28 Cattin-Ortolá, J. *et al.* Sequences in the cytoplasmic tail of SARS-CoV-2 Spike facilitate expression at the cell surface and syncytia formation. *bioRxiv*, 2020.2010.2012.335562, doi:10.1101/2020.10.12.335562 (2021).
29 Meng, B. *et al.* Recurrent emergence and transmission of a SARS-CoV-2 spike deletion H69/V70 and role in Alpha Variant B.1.1.7. *Cell reports*, doi:https://doi.org/10.1016/j.celrep.2021.109292 (2021).
30 Winstone, H. *et al.* The Polybasic Cleavage Site in SARS-CoV-2 Spike Modulates Viral Sensitivity to Type I Interferon and IFITM2. *Journal of virology* **95**, e02422-02420, doi:10.1128/jvi.02422-20 (2021).
31 Kemp, S. *et al.* Recurrent emergence and transmission of a SARS-CoV-2 Spike deletion H69/V70. *bioRxiv*, 2020.2012.2014.422555, doi:10.1101/2020.12.14.422555 (2021).
32 Peacock, T. P. *et al.* The furin cleavage site of SARS-CoV-2 spike protein is a key determinant for transmission due to enhanced replication in airway cells. *bioRxiv* (2020).
33 Kemp, S. A. *et al.* SARS-CoV-2 evolution during treatment of chronic infection. *Nature*, doi:10.1038/s41586-021-03291-y (2021).
34 Meng, B. *et al.* Recurrent emergence of SARS-CoV-2 spike deletion H69/V70 and its role in the variant of concern lineage B.1.1.7. *Cell Reports*, 109292, doi:https://doi.org/10.1016/j.celrep.2021.109292 (2021).
35 Bhoyar, R. C. *et al.* High throughput detection and genetic epidemiology of SARS-CoV-2 using COVIDSeq next-generation sequencing. *PloS one* **16**, e0247115, doi:10.1371/journal.pone.0247115 (2021).
36 Bernal, J. L. *et al.* Effectiveness of COVID-19 vaccines against the B.1.617.2 variant. *medRxiv*, 2021.2005.2022.21257658, doi:10.1101/2021.05.22.21257658 (2021).
37 Malani, A. *et al.* Seroprevalence of SARS-CoV-2 in slums versus non-slums in Mumbai, India. *Lancet Glob Health* **9**, e110-e111, doi:10.1016/S2214-109X(20)30467-8 (2021).
38 Wall, E. C. *et al.* Neutralising antibody activity against SARS-CoV-2 VOCs B.1.617.2 and B.1.351 by BNT162b2 vaccination. *Lancet*, doi:10.1016/S0140-6736(21)01290-3 (2021).
39 Planas, D. *et al.* Reduced sensitivity of infectious SARS-CoV-2 variant B.1.617.2 to monoclonal antibodies and sera from convalescent and vaccinated individuals. *bioRxiv*, 2021.2005.2026.445838, doi:10.1101/2021.05.26.445838 (2021).
40 Lempp, F. A. *et al.* Membrane lectins enhance SARS-CoV-2 infection and influence the neutralizing activity of different classes of antibodies. *bioRxiv*, 2021.2004.2003.438258, doi:10.1101/2021.04.03.438258 (2021).
41 McCarthy, K. R. *et al.* Natural deletions in the SARS-CoV-2 spike glycoprotein drive antibody escape. *Science* (2020).
42 McCallum, M. *et al.* N-terminal domain antigenic mapping reveals a site of vulnerability for SARS-CoV-2. *Cell* **184**, 2332-2347 e2316, doi:10.1016/j.cell.2021.03.028 (2021).

43 Zeng, C. *et al.* SARS-CoV-2 Spreads through Cell-to-Cell Transmission. *bioRxiv*, 2021.2006.2001.446579, doi:10.1101/2021.06.01.446579 (2021).
44 Jackson, L. *et al.* SARS-CoV-2 cell-to-cell spread occurs rapidly and is insensitive to antibody neutralization. *bioRxiv*, 2021.2006.2001.446516, doi:10.1101/2021.06.01.446516 (2021).
45 Peacock, T. P. *et al.* The furin cleavage site in the SARS-CoV-2 spike protein is required for transmission in ferrets. *Nat Microbiol* **6**, 899-909, doi:10.1038/s41564-021-00908-w (2021).
46 Johnson, B. A. *et al.* Loss of furin cleavage site attenuates SARS-CoV-2 pathogenesis. *Nature* **591**, 293-299, doi:10.1038/s41586-021-03237-4 (2021).
47 Braga, L. *et al.* Drugs that inhibit TMEM16 proteins block SARS-CoV-2 Spike-induced syncytia. *Nature*, doi:10.1038/s41586-021-03491-6 (2021).
48 Planas, D. *et al.* Reduced sensitivity of SARS-CoV-2 variant Delta to antibody neutralization. *Nature*, doi:10.1038/s41586-021-03777-9 (2021).
49 Group, R. C. *et al.* Casirivimab and imdevimab in patients admitted to hospital with COVID-19 (RECOVERY): a randomised, controlled, open-label, platform trial. *medRxiv*, 2021.2006.2015.21258542, doi:10.1101/2021.06.15.21258542 (2021).
50 Kemp, S. A. *et al.* SARS-CoV-2 evolution during treatment of chronic infection. *Nature* **592**, 277-282, doi:10.1038/s41586-021-03291-y (2021).
51 Shinde, V. *et al.* Efficacy of NVX-CoV2373 Covid-19 Vaccine against the B.1.351 Variant. *New England Journal of Medicine*, doi:10.1056/NEJMoa2103055 (2021).
52 Abu-Raddad, L. J., Chemaitelly, H. & Butt, A. A. Effectiveness of the BNT162b2 Covid-19 Vaccine against the B.1.1.7 and B.1.351 Variants. *New England Journal of Medicine*, doi:10.1056/NEJMc2104974 (2021).
53 Sadoff, J. *et al.* Safety and Efficacy of Single-Dose Ad26.COV2.S Vaccine against Covid-19. *New England Journal of Medicine*, doi:10.1056/NEJMoa2101544 (2021).
54 Endo, A., Centre for the Mathematical Modelling of Infectious Diseases, C.-W. G., Abbott, S., Kucharski, A. J. & Funk, S. Estimating the overdispersion in COVID-19 transmission using outbreak sizes outside China. *Wellcome Open Res* **5**, 67, doi:10.12688/wellcomeopenres.15842.3 (2020).
55 Katoh, K. & Standley, D. M. MAFFT multiple sequence alignment software version 7: improvements in performance and usability. *Mol Biol Evol* **30**, 772-780, doi:10.1093/molbev/mst010 (2013).
56 Minh, B. Q. *et al.* IQ-TREE 2: New models and efficient methods for phylogenetic inference in the genomic era. *bioRxiv*, 849372, doi:10.1101/849372 (2019).
57 Yu, G., Smith, D. K., Zhu, H., Guan, Y. & Lam, T. T. Y. ggtree: an R package for visualization and annotation of phylogenetic trees with their covariates and other associated data. *Methods in Ecology and Evolution* **8**, 28-36 (2017).
58 Shu, Y. & McCauley, J. GISAID: Global initiative on sharing all influenza data - from vision to reality. *Euro surveillance : bulletin Europeen sur les maladies transmissibles = European communicable disease bulletin* **22**, 30494, doi:10.2807/1560-7917.ES.2017.22.13.30494 (2017).
59 Wrobel, A. G. *et al.* SARS-CoV-2 and bat RaTG13 spike glycoprotein structures inform on virus evolution and furin-cleavage effects. *Nat Struct Mol Biol* **27**, 763-767, doi:10.1038/s41594-020-0468-7 (2020).
60 Rihn, S. J. *et al.* A plasmid DNA-launched SARS-CoV-2 reverse genetics system and coronavirus toolkit for COVID-19 research. *PLoS Biol* **19**, e3001091, doi:10.1371/journal.pbio.3001091 (2021).
61 Vermeire, J. *et al.* Quantification of reverse transcriptase activity by real-time PCR as a fast and accurate method for titration of HIV, lenti- and retroviral vectors. *PloS one* **7**, e50859-e50859, doi:10.1371/journal.pone.0050859 (2012).
62 Matsuyama, S. *et al.* Enhanced isolation of SARS-CoV-2 by TMPRSS2-expressing cells. *Proc Natl Acad Sci U S A* **117**, 7001-7003, doi:10.1073/pnas.2002589117 (2020).

63 Reed, L. J. & Muench, H. A Simple Method of Estimating Fifty Percent Endpoints. *Am J Hygiene* **27**, 493-497 (1938).
64 Motozono, C. *et al.* SARS-CoV-2 spike L452R variant evades cellular immunity and increases infectivity. *Cell Host Microbe*, doi:10.1016/j.chom.2021.06.006 (2021).
65 Shema Mugisha, C. *et al.* A simplified quantitative real-time PCR assay for monitoring SARS-CoV-2 growth in cell culture. *mSphere* **5**, doi:10.1128/mSphere.00658-20 (2020).
66 Schmidt, F. *et al.* Measuring SARS-CoV-2 neutralizing antibody activity using pseudotyped and chimeric viruses. 2020.2006.2008.140871, doi:10.1101/2020.06.08.140871 %J bioRxiv (2020).
67 Mlcochova, P. *et al.* Combined point of care nucleic acid and antibody testing for SARS-CoV-2 following emergence of D614G Spike Variant. *Cell Rep Med*, 100099, doi:10.1016/j.xcrm.2020.100099 (2020).
68 Ou, X. *et al.* Characterization of spike glycoprotein of SARS-CoV-2 on virus entry and its immune cross-reactivity with SARS-CoV. *Nat Commun* **11**, 1620, doi:10.1038/s41467-020-15562-9 (2020).
69 Kodaka, M. *et al.* A new cell-based assay to evaluate myogenesis in mouse myoblast C2C12 cells. *Experimental cell research* **336**, 171-181 (2015).
70 Papa, G. *et al.* Furin cleavage of SARS-CoV-2 Spike promotes but is not essential for infection and cell-cell fusion. *PLoS Pathogens* **17**, e1009246 (2021).
71 Buchrieser, J. *et al.* Syncytia formation by SARS-CoV-2-infected cells. *The EMBO journal* **39**, e106267 (2020).

INSACOG CONSORTIUM MEMBERS

NIBMG: Saumitra Das, Arindam Maitra, Sreedhar Chinnaswamy, Nidhan Kumar Biswas;

ILS: Ajay Parida, Sunil K Raghav, Punit Prasad;

InSTEM/ NCBS: Apurva Sarin, Satyajit Mayor, Uma Ramakrishnan, Dasaradhi Palakodeti, Aswin Sai Narain Seshasayee;

CDFD: K Thangaraj, Murali Dharan Bashyam, Ashwin Dalal;

NCCS: Manoj Bhat, Yogesh Shouche, Ajay Pillai;

IGIB: Anurag Agarwal, Sridhar Sivasubbu, Vinod Scaria;

NIV: Priya Abraham, Potdar Varsha Atul, Sarah S Cherian;

NIMHANS: Anita Sudhir Desai, Chitra Pattabiraman, M. V. Manjunatha, Reeta S Mani, Gautam Arunachal Udupi;

NCDC: Sujeet Singh, Himanshu Chauhan, Partha Rakshit, Tanzin Dikid;

CCMB: Vinay Nandicoori, Karthik Bharadwaj Tallapaka, Divya Tej Sowpati

INSACOG collaborating divisions and clinical partners

Biotechnology division, NCDC: Hema Gogia, Hemlata Lall, Kalaiarasan Ponnusamy, Kaptan Verma, Mahesh S Dhar, Manoj K Singh, Meena Datta, Namita Soni, Namonarayan

Meena, Partha Rakshit, Preeti Madan, Priyanka Singh, Radhakrishnan V. S, Ramesh Sharma, Rajeev Sharma, Robin Marwal, Sandhya Kabra, Sattender Kumar, Swati Kumari, Uma Sharma, Urmila Chaudhary

Integrated Disease Surveillance Program (IDSP), NCDC, Central and State IDSP units

Centre of Epidemiology, NCDC

Sri Ganga Ram Hospital, Rajinder Nagar, New Delhi: Dept of Clinical Microbiology & Immunology and Director Medical Hospital Administration, Chand Wattal, J K Oberoi, Neeraj Goel, Reena Raveendran, S. Datta

Northern Railway Central Hospital, Basant Lane, New Delhi: Meenakshi Agarwal

Indraprastha Apollo Hospitals, New Delhi: Administration and Microbiology department, Raju Vaishya

The Genotype to Phenotype Japan (G2P-Japan) Consortium members

The Institute of Medical Science, The University of Tokyo: Jumpei Ito, Izumi Kimura, Keiya Uriu, Yusuke Kosugi, Mai Suganami, Akiko Oide, Miyabishara Yokoyama, Mika Chiba

Hiroshima University: Ryoko Kawabata, Nanami Morizako

Tokyo Metropolitan Institute of Public Health: Kenji Sadamasu, Hiroyuki Asakura, Mami Nagashima, Kazuhisa Yoshimura

University of Miyazaki: Akatsuki Saito, Erika P Butlertanaka, Yuri L Tanaka

Kumamoto University: Terumasa Ikeda, Chihiro Motozono, Hesham Nasser, Ryo Shimizu, Yue Yuan, Kazuko Kitazato, Haruyo Hasebe

Tokai University: So Nakagawa, Jiaqi Wu, Miyoko Takahashi

Hokkaido University: Takasuke Fukuhara, Kenta Shimizu, Kana Tsushima, Haruko Kubo

Kyoto University: Kotaro Shirakawa, Yasuhiro Kazuma, Ryosuke Nomura, Yoshihito Horisawa, Akifumi Takaori-Kondo

National Institute of Infectious Diseases: Kenzo Tokunaga, Seiya Ozono

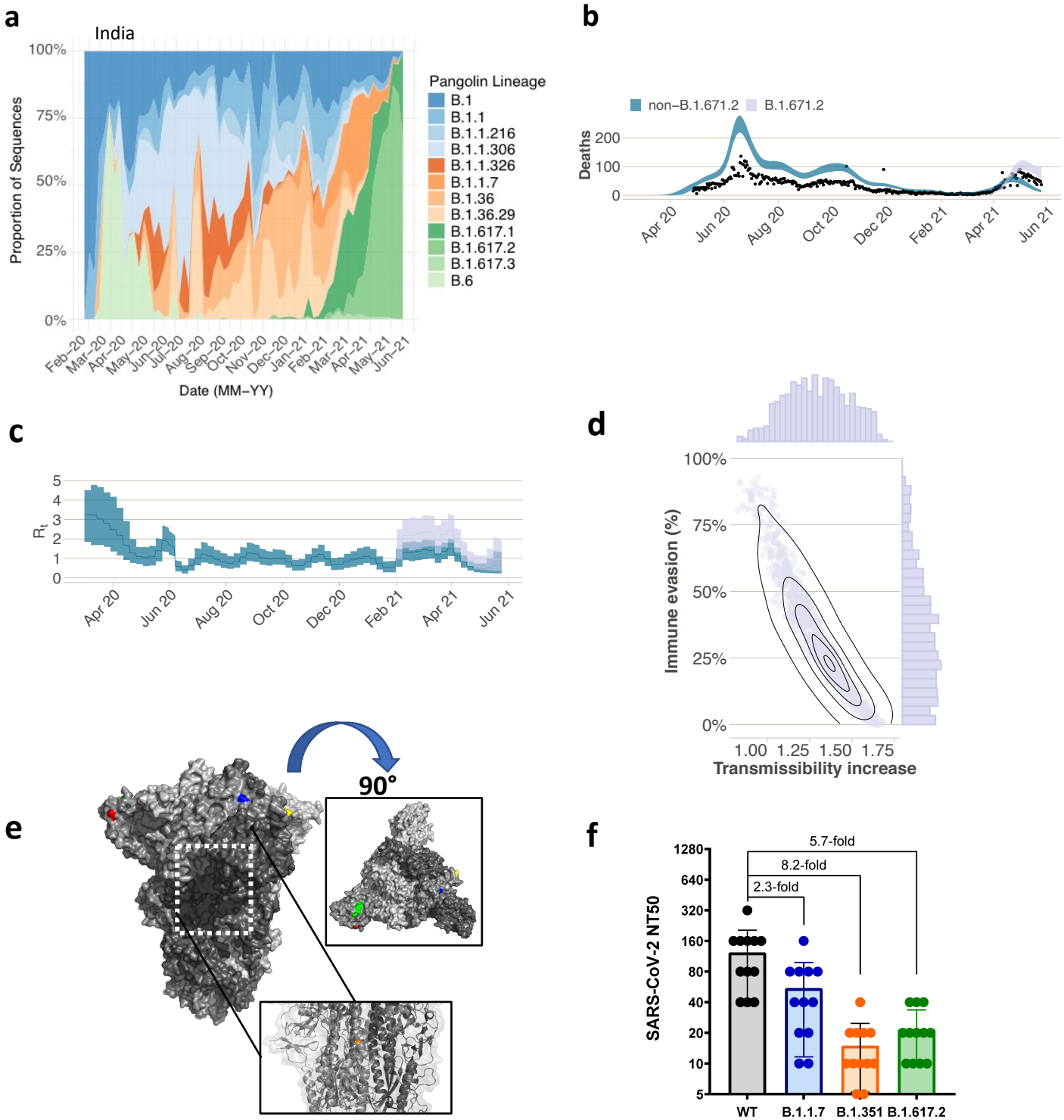

Figure. 1. **Rapid Expansion of Delta variant B.1.617.2 in India with immune evasion and increased transmissibility a.** Proportion of lineages in incident cases of SARS-CoV-2 in India 2020-2021. **b-d**. Modelling resurgence of SARS-CoV-2 transmission in Mumbai and the epidemiological characteristics of B.1.617.2, inferred using a two category Bayesian transmission model[1] fitted to COVID-19 mortality, serological and genomic sequence data. The introduction date for B.1.671.2 is set to 31st Jan 2021 and 50% under-reporting in COVID-19 mortality data is assumed. **b.** Daily incidence of COVID-19 mortality with black dots showing the observed data. Coloured lines show the mean of posterior estimates of true number of deaths (i.e. after accounting for 50% underreporting) and shaded region representing the 95% CI. **c.** Bayesian posterior estimates of trends in the reproduction number (R_t) for the B.1.671.2 and non- B.1.671.2 variant categories**. d.** Joint posterior distribution of the inferred transmissibility increase and degree of immune evasion (predominantly re-infection in India due to low vaccination coverage) for B.1.671.2 (relative to non- B.1.671.2 categories). Grey contours refer to posterior density intervals ranging from the 95% and 5% isoclines. Marginal posterior distributions for each parameter shown along each axis. **e.** Surface representation of the SARS-CoV-2 B.1.671.2 Spike trimer (PDB: 6ZGE). L19R (red), del157/158 (green) L452R (blue) and T478K (yellow). The white dashed box indicates the location of the D950N (orange) **f. Neutralization of Delta variant by convalescent human serum from mid-2020** in Vero-hACE2 TMPRSS2 cells. Fold-change in serum neutralisation 100 $TCID_{50}$ of B.1.17 (Alpha), B.1.351 (Beta) and B.1617.2 (Delta) variants relative to wild-type (IC19), n=12.

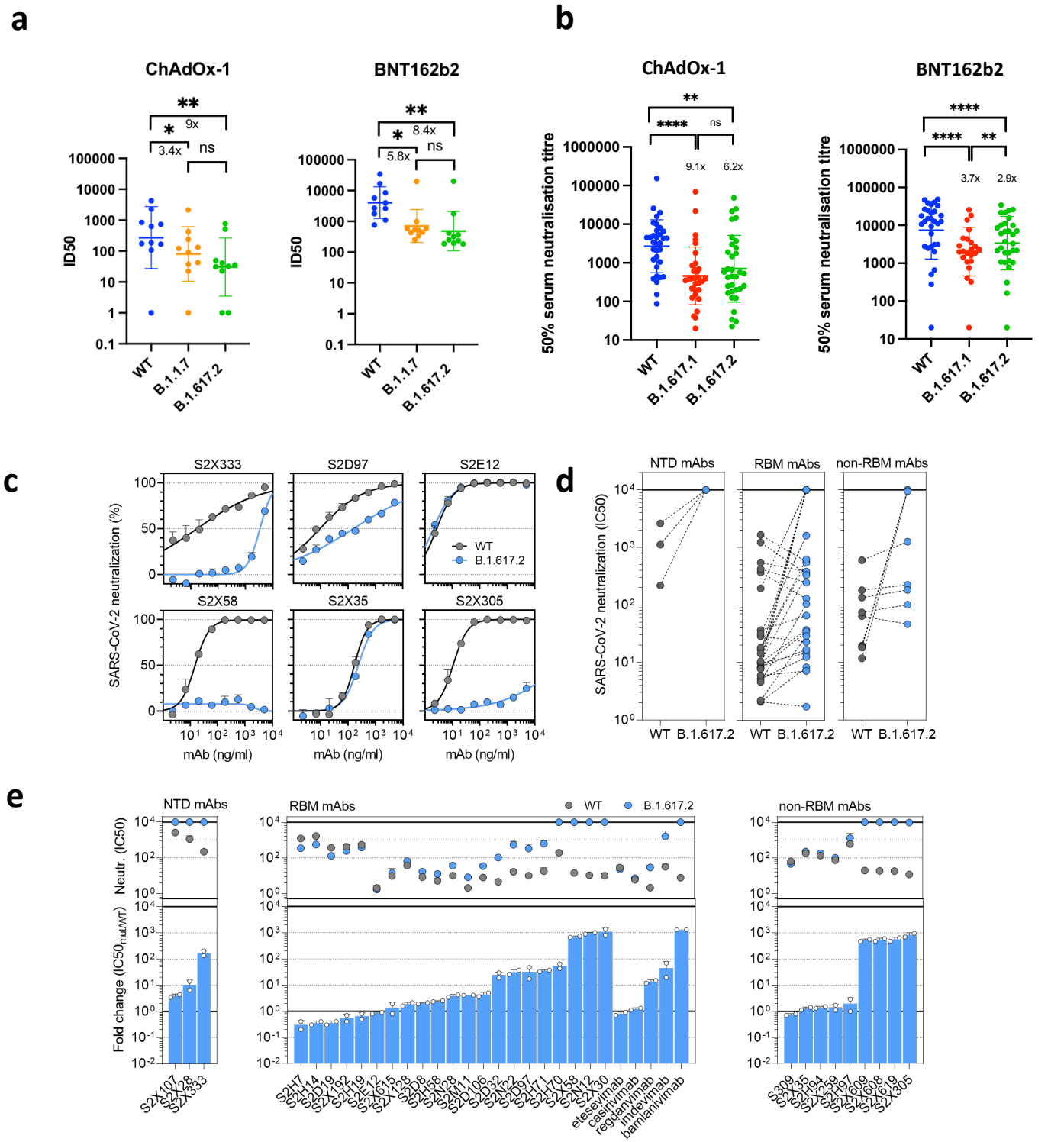

Figure 2: Delta variant B.1.617.2 shows reduced sensitivity to neutralizing antibodies from sera derived following vaccination and to monoclonal antibodies. a. Neutralisation of delta variant live virus isolate by sera from vaccinated individuals (n=10 ChAdOx-1 or n=10 BNT12b2) in comparison to B.1.1.7 and Wuhan-1 wild type (WT). **5**-fold dilutions of vaccinee sera were mixed with wild type (WT) or viral variants (MOI 0.1) for 1h at 37˚C. Mixture was added to Vero-hACE2/TMPRSS2 cells for 72h. Cells were fixed and stained with Coomasie blue and % of survival calculated. ID50 were calculated using nonlinear regression. Graph represents average of two independent experiments.**b.** Neutralisation of B.1.617 spike pseudotyped virus (PV) and wild type (WT, Wuhan-1 D614G) by vaccine sera (n=33 ChAdOx-1 or n=32 BNT162b2). GMT (geometric mean titre) with s.d are presented. Data representative of two independent experiments each with two technical replicates. **p<0.01, *** p<0.001, ****p<0.0001 Wilcoxon matched-pairs signed rank test, ns not significant. **c.** Neutralisation of WT D614 (black) and B.1.617.2 mutant (blue) pseudotyped SARS-CoV-2-VSV by 6 selected mAbs from one representative experiment out of 2 independent experiments. S2X333 is an NTD-specific mAb, S2D97, S2E12 and S2X58 are RBM-specific mAbs, while S2X35 and S2X305 are non-RBM mAbs. **d.** Neutralisation of WT and B.1.617.2 VSV by 38 mAbs targeting NTD (n=3), RBM (n=26) and non-RBM (n=9). Shown are the mean IC50 values (ng/ml) from 2 independent experiments. Non-neutralising IC50 titers were set at 10^4 ng/ml. **e**. Neutralisation shown as mean IC50 values (upper panel) and average fold change of B.1.617.2 relative to WT (lower panel) of 38 mAbs tested in 2 independent experiments, including 5 clinical-stage mAbs tested using Vero E6 cells expressing TMPRSS2.

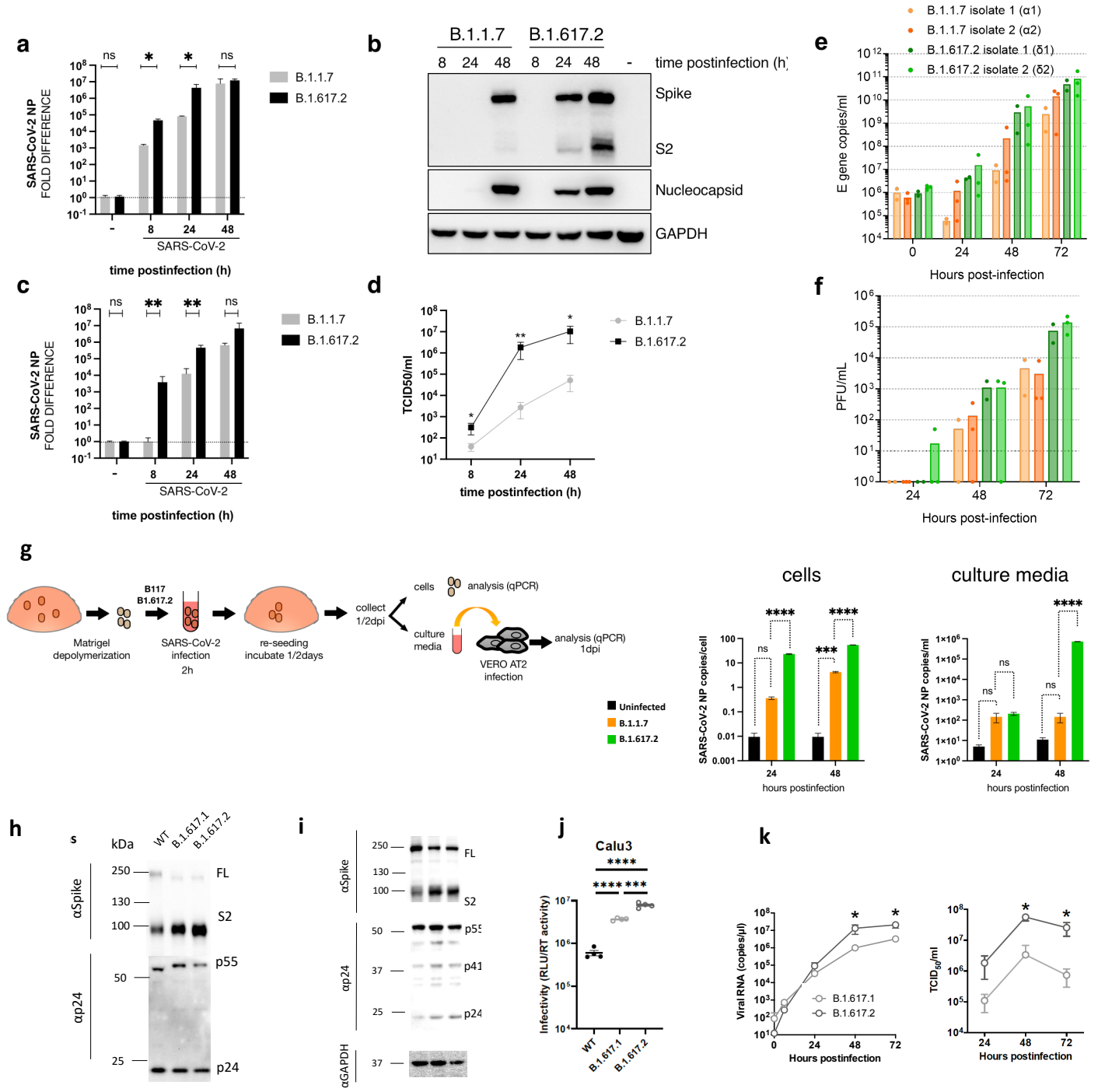

Figure 3. a. **SARS-CoV-2 B.1.617.2 Delta Variant replication and and spike mediated entry efficiency. a-d**. Live virus replication in CaLu-3 lung cells comparing B.1.1.7 with B.1.617.2. Calu3 cells were infected with variants at MOI 0.1. Cells and supernatants containing released virus were collected for RNA isolation, western blot and TCID50 at 8, 24 and 48h post-infection. **a.** viral loads were measured by qPCR in cell lysates. **b.** viral protein levels were detected in cell lysates. **c-d** Live virus produced from infected Calu3 cells was collected and used to infect permissive Vero Ace2/TMPRSS2 cells to measure **c**. viral loads in Vero cells or **d**. to measure TCID50/ml. **e-f.** Virus replication kinetics in human airway epithelial (HAE) system with air liquid interface ALI, using two B.1.617.2 isolates and two B.1.1.7 isolates. **g.** Live virus **r**eplication in airway epithelial organoid cultures. Airway epithelial organoids were infected with SARS-CoV-2 variants B.1.1.7 and B.1.617.2 at MOI 1. Cells were lysed 24 and 48h post-infection and total RNA isolated. qPCR was used to determine copies of nucleoprotein gene in organoid cells and infectivity of cell free virus measured by infection of Vero AT2 cells. Data represent are representative of two independent experiments. **h** and **i.** western blots of pseudotyped virus (PV) virions (h) and cell lysates (i) of 293T producer cells following transfection with plasmids expressing lentiviral vectors and SARS-CoV-2 S B.1.617.1 and Delta variant B.1.617.2 versus WT (Wuhan-1 with D614G), probed with antibodies for HIV-1 p24 and SARS-Cov-2 S2. **j.** Single round infectivity on Calu-3 by spike B.1.617.2 and B.1.617.1 versus WT D614G parental plasmid PV produced in 293T cells. Data are representative of three independent experiments. **k.** Growth kinetics of B.1.617.1 and B.1.617.2 variants. Viral isolates of B.1.617.1 and B.1.617.2 [200 50% tissue culture infectious dose ($TCID_{50}$)] were inoculated into Calu-3 cells and the copy number of viral RNA in the culture supernatant was quantified by real-time RT-PCR over time. $TCID_{50}$ of released virus in supernatant was also measured over time. Assays were performed in quadruplicate. *, $P<0.05$ by Mann-Whitney U test.. ns, non-significant; * $p<0.05$; ** $p < 0.01$. ***$p<0.001$, ****$p<0.0001$ (-) uninfected cells. Data are representative of two independent experiments

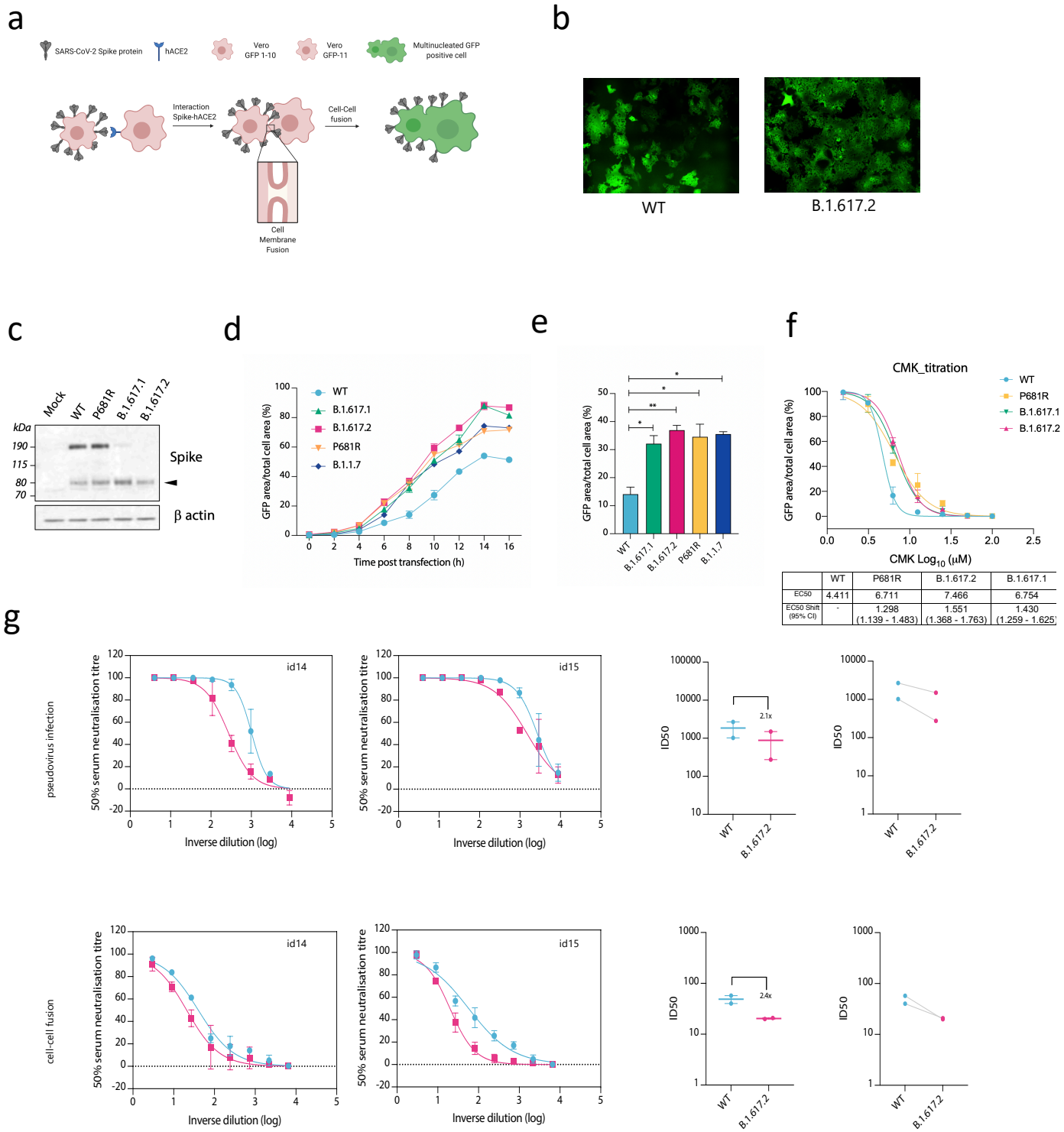

	WT	P681R	B.1.617.2	B.1.617.1
EC50	4.411	6.711	7.466	6.754
EC50 Shift (95% CI)	-	1.298 (1.139 - 1.483)	1.551 (1.368 - 1.763)	1.430 (1.259 - 1.625)

Figure 4: B.1.617.2 Delta variant spike confers accelerated cell-cell fusion activity that can be blocked by anti-spike neutralising antibodies in sera. a. Schematic of cell-cell fusion assay. **b.** Reconstructed images at 10 hours of GFP positive syncytia formation. Scale bars represent 400 mm. c. western blot of cell lysates 48 hours after transfection of spike plasmids. Anti-S2 antibody. **d,e.** Quantification of cell-cell fusion kinetics showing percentage of green area to total cell area over time. Mean is plotted with error bars representing SEM**. f**. Sensitivity of fusion kinetics to furin inhibitor CMK as shown by titration of drug and measurement of fusion after 10hrs. Mean is plotted with error bars representing SEM. **g**. comparison of impact of post vaccine sera (n=2) on PV neutralisation (top) and cell-cell fusion (bottom), comparing WT and Delta variant B.1.671.2. Data are representative of at least two independent experiments.

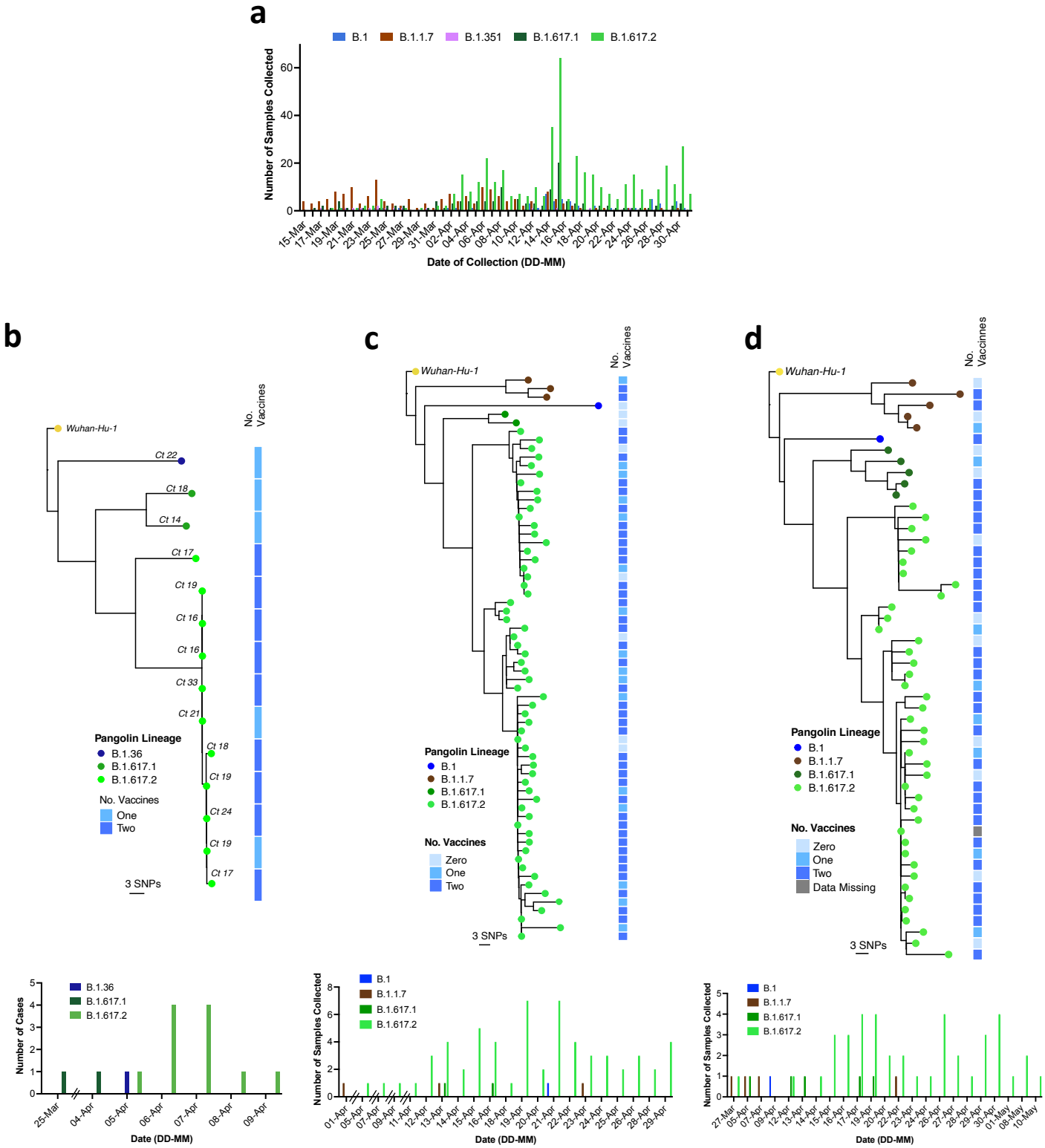

Figure 5. SARS-CoV-2 B.1.617.2 infection in vaccinated health care workers. a. Case frequencies of five most commonly occurring SARS CoV-2 lineages over a six week period from March to April 2021 for Delhi. **b-d** Maximum likelihood phylogenies of vaccine breakthrough SARS-CoV-2 sequences amongst vaccinated HCW at three centres are presented. Phylogenies were inferred with IQTREE2 with 1000 bootstrap replicates. Trees are rooted on Wuhan-Hu-1 and annotated with the lineage designated by pangolin v.2.4.2. The number of COVISHIELD (ChAdOx-1) vaccinations received by each individual is indicated by the heatmap to the right. White space indicates missing data. At the bottom of each tree is a case frequency graph by date of testing.

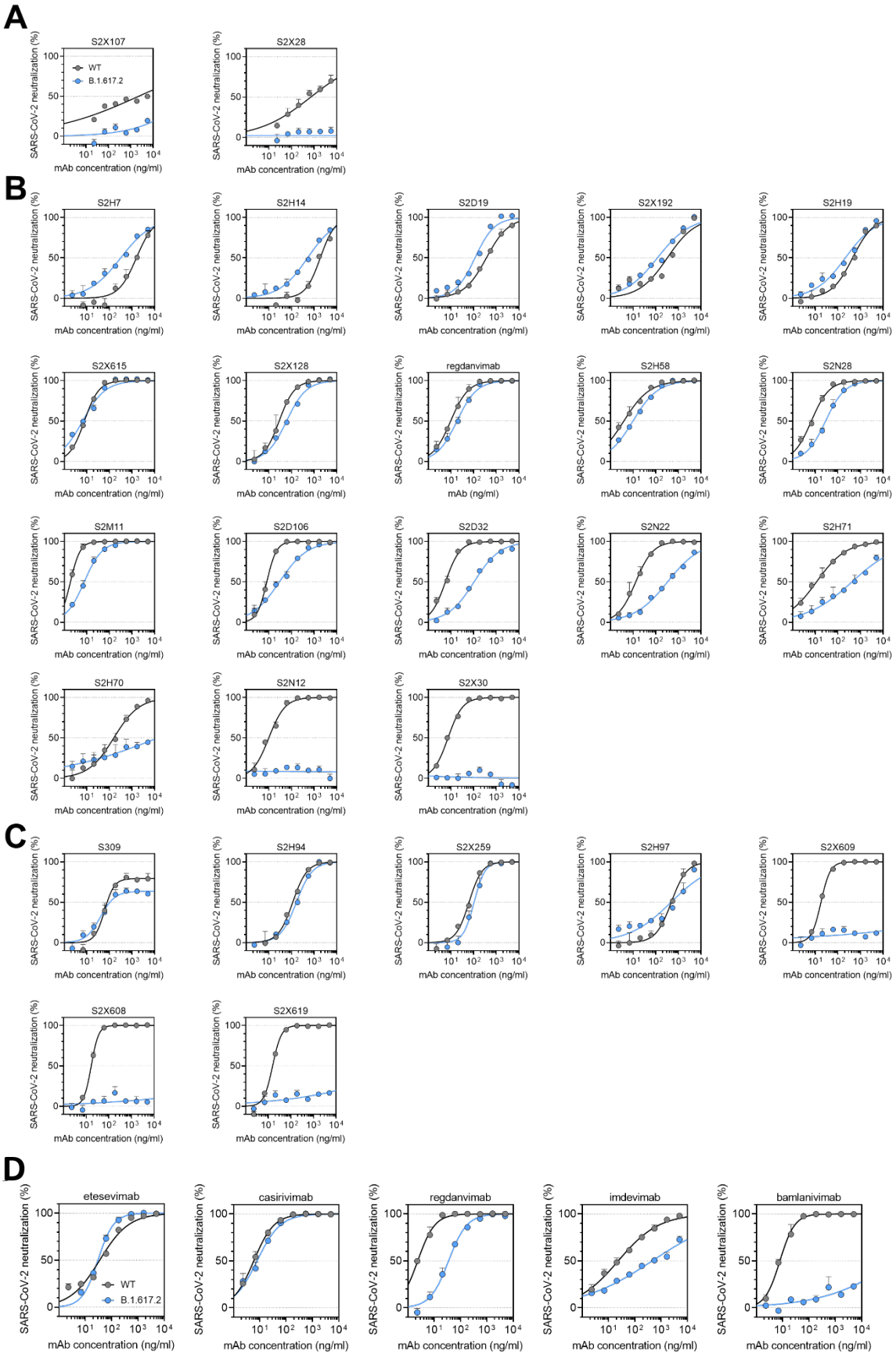

Extended Data Figure 1. Neutralisation by a panel of NTD- and RBD-specific mAbs against WT and B.1.617.2 mutant SARS-CoV-2 pseudotyped viruses. a-c, Neutralisation of WT (Wuhan-1 D614, black) and B.1.617.2 mutant (blue) pseudotyped SARS-CoV-2-VSV by 27 mAbs targeting NTD (A, n=3), RBM (B, n=18) and non-RBM (C, n=7). Shown is one representative experiment out of 2 independent experiments. **d. Neutralisation by 5 RBM clinical-stage mAbs against WT and B.1.617.2 mutant SARS-CoV-2 pseudotyped viruses.** Neutralisation of WT (black) and B.1.617.2 mutant (blue) pseudotyped SARS-CoV-2-VSV by 5 clinical-stage mAbs using Vero E6 cells expressing TMPRSS2.

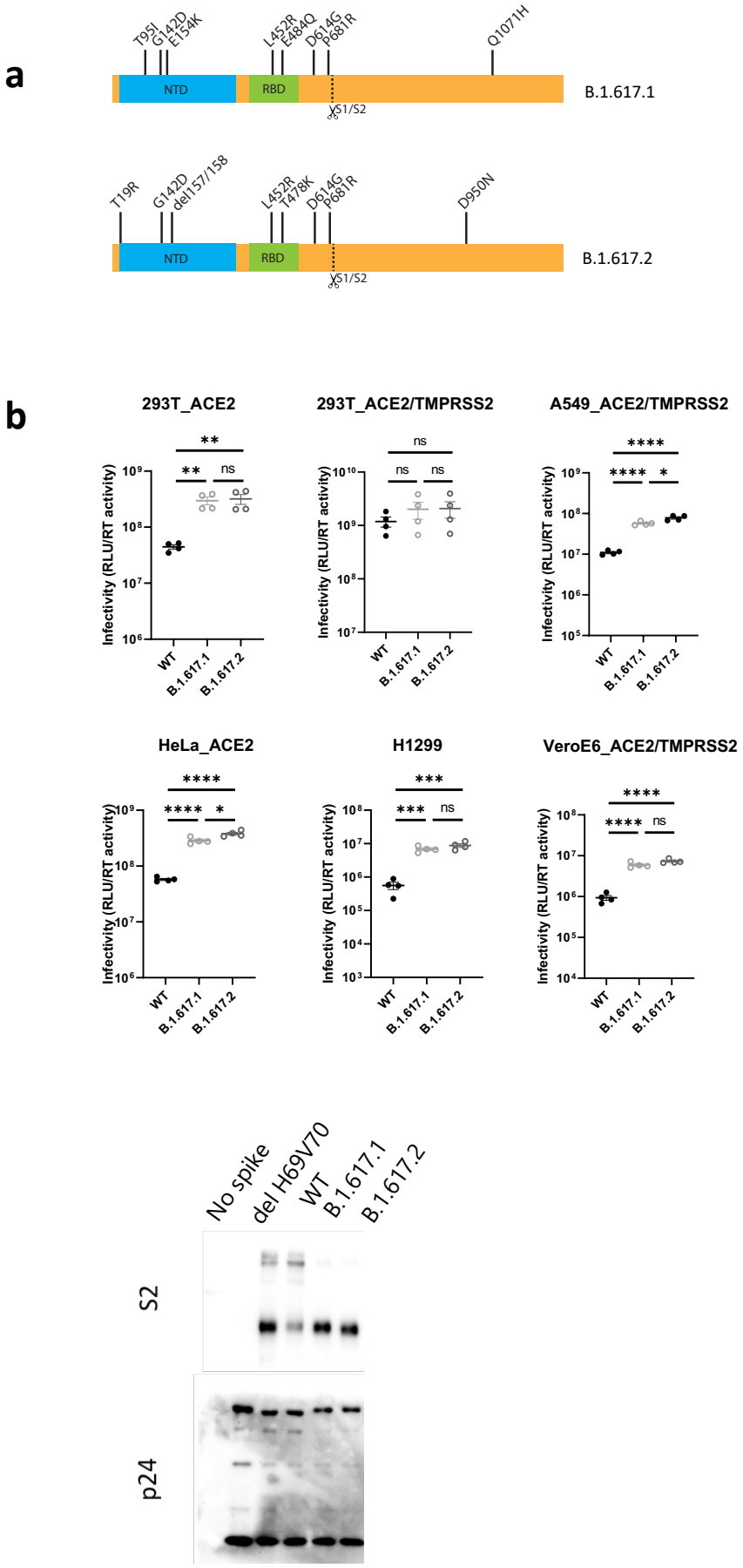

Extended Data Figure 2: B.1.617.2 spike confers increased cell entry. a. diagram showing mutations present in spike plasmids used for cell entry PV experiments **b.** Single round infectivity on different cell targets by spike B.1.617.1 and B.1.617.1 versus WT (Wuhan-1 D614G) PV produced in 293T cells. Data are representative of three independent experiments. Statistics were performed using unpaired Student t test. c. Representative western blotting of supernatants from transfected 293T probing for S2 and p24 in PV.

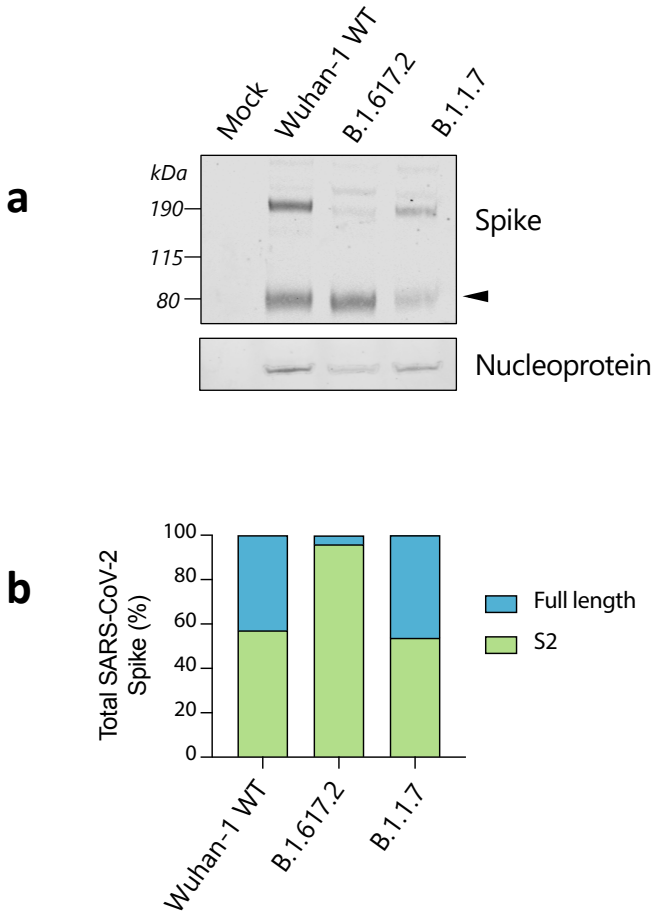

Extended Data Figure 3. Spike cleavage in B.1.617.2 virions compared to B.1.17. a. Representative western blot analysis of spike and nucleoprotein present in SARS-CoV-2 particles from the indicated viruses produced in Vero-hACE2-TMPRS22 cells 48 hours post infection. The arrowhead identifies the S2 subunit. b. Quantification of cleaved and full-length spike of the indicated viruses.

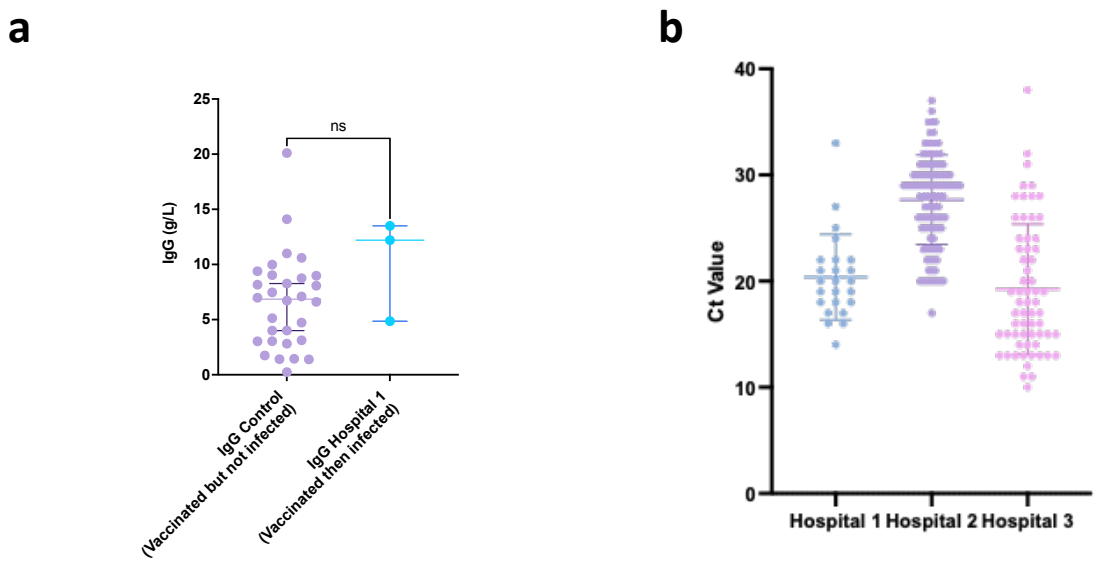

Extended Data Figure 4. Breakthrough SARS-CoV-2 infections amongst vaccinated health care workers (HCW) a. Comparison of IgG antibody titres between a control group of vaccinated individuals receiving two doses of ChadOx-1 who have not been infected with SARS-CoV-2, with vaccinated healthcare workers who had received two doses and subsequently tested positive for SARS-CoV-2. b. Ct values in nose/throat swabs testing positive by hospital. Bars represent Mean and 95% CI.

Extended Data Table 1A. Sensitivity analysis for the two-category model: B.1.617.2 and non-B.1.617.2 lineages under different combinations of B.1.617.2 lineage introduction dates and differing extents of mortality underreporting. The inferred changes in epidemiological characteristics of B.1.617.2 are presented via the estimated posterior mean and Bayesian 50% credible interval. Transmissibility increase is compared to co-circulating lineages in Mumbai.

Starting Date	Under-Reporting Of Deaths	Evasion of protection from previous SARS-CoV-2 Infections (%)	Transmissibility Increase of B.1.617.2*
31st Jan 2021	**30%**	32% (18%-48%)	2% (-19%-18%)
	50%	38% (16%-55%)	26% (11%-42%)
	70%	35% (17%-50%)	39% (29%-51%)
1st Jan 2021	**30%**	17% (9%-25%)	18% (0%-35%)
	50%	24% (7%-34%)	34% (20%-50%)
	70%	32% (19%-45%)	37% (28%-47%)
15th Dec 2020	**30%**	10% (5%-15%)	28% (17%-42%)
	50%	28% (11%-39%)	27% (16%-41%)
	70%	26% (9%-38%)	40% (31%-50%)
1st Dec 2020	**30%**	5% (3%-7%)	39% (31%-47%)
	50%	14% (4%-21%)	40% (33%-50%)
	70%	24% (9%-35%)	39% (31%-49%)

Extended Data Table 1B. Sensitivity of the inferred increase in transmissibility and evasion of cross-immunity of the B.1.617.2 lineage, under varying transmissibility increase prior assumptions. Transmissibility increase is compared to co-circulating lineages in Mumbai. The estimated posterior mean and Bayesian 50% credible interval is shown for all inferred characteristics.

Transmissibility increase prior	Evasion of protection from previous SARS-CoV-2 Infections (%)	Transmissibility Increase of B.1.617.2*
LogNormal(0,0.25)	33% (13%-54%)	27% (16%-48%)
Gamma(5,5)	38% (16%-55%)	26% (11%-42%)
Normal^{+}(1,1)	29% (13%-43%)	44% (35%-54%)

Extended Data Table 1C. Sensitivity of the inferred increase in transmissibility and evasion of cross-immunity of the B.1.617.2 lineage, under varying cross-immunity prior assumptions. Transmissibility increase is compared to co-circulating lineages in Mumbai. The under reporting is 50% and starting date is 31st Jan 2021, same as in Figure 1(b). The results are presented as the estimated posterior mean and Bayesian 50% credible interval.

Degree of Cross-protection prior	Evasion of protection from previous SARS-CoV-2 Infections (%)	Transmissibility Increase from B.1.617.2*
Beta(2,1)	38% (16%-55%)	26% (11%-42%)
Beta(3,1)	25% (11%-35%)	47% (40%-55%)
Beta(4,1)	23% (7%-33%)	48% (41%-57%)
Beta(5,1)	16% (6%-24%)	52% (47%-59%)

Extended Data Table 2 Demographic information for individuals undergoing two dose SARS-CoV-2 vaccination with ChAdOx-1 or BNT162b2

	ChAdOx-1 (N=33)	BNT162b2 (N=32)	P. value
Female (*%*)	18 (54.5)	13 (40.6)	0.38[a]
Median Age *Years* (IQR)	67 (64 - 71)	71 (46 -83)	0.74[b]
Median time *in Days* since dose 2 (IQR)	31 (21 -38)	27 (24 -29)	0.15[b]
Serum Geometric Mean Titre *GMT* for delta variant (95% CI)	654 (313 -1365)	3372 (1856 - 6128)	0.0006[b]
Serum Geometric Mean Titre *GMT* for WT (95% CI)	2625 (1492 - 4618)	7393 (3893 - 14041)	0.0030[b]

[a]Chi-square test, [b] Mann-Whitney test

mAb	Domain/site	IC50 WT (ng/ml)	IC50 B.1.617.2 (ng/ml)	VH usage (% id.)	Source (DSO)	ACE2 blocking	Ref.
S2X107	**NTD**	2611.00	10000.00	4-38-2 (97)	Sympt. (75)	Neg.	McCallum et al.
S2X28	**NTD**	1121.30	10000.00	3-30 (97.9)	Sympt. (48)	Neg.	McCallum et al.
S2X333	**NTD**	217.95	35016.00	3-33 (96.5)	Sympt. (125)	Neg.	McCallum et al.
S2H7	**RBM**	1227.25	347.05	3-66 (98.3)	Sympt. (17)	Weak	Thomson et al.
S2H14	**RBM**	1666.00	566.40	3-15 (100)	Sympt. (17)	Weak	Piccoli et al.; Thomson et al.
S2D19	**RBM**	369.55	129.95	4-31 (99.7)	Hosp. (49)	Moderate	Thomson et al.
S2X192	**RBM**	423.00	246.15	1-69 (96.9)	Sympt. (75)	Weak	Thomson et al.
S2H19	**RBM**	549.25	382.45	3-15 (98.6)	Sympt. (45)	Weak	Thomson et al.
S2E12	**RBM**	2.09	1.72	1-58 (97.6)	Hosp. (51)	Strong	Thomson et al.; Tortorici et al.
S2X615	**RBM**	9.80	14.59	3-11 (94.8)	Sympt. (271)	Strong	Collier et al.
S2X128	**RBM**	36.82	65.97	1-69-2 (97.6)	Sympt. (75)	Strong	Thomson et al.
S2D8	**RBM**	8.44	16.78	3-23 (96.5)	Hosp. (49)	Strong	Thomson et al.
S2H58	**RBM**	5.21	12.55	1-2 (97.9)	Sympt. (45)	Strong	Thomson et al.
S2N28	**RBM**	10.05	36.95	3-30 (97.2)	Hosp. (51)	Strong	Thomson et al.
S2M11	**RBM**	2.07	8.32	1-2 (96.5)	Hosp. (46)	Weak	Thomson et al.; Tortorici et al.
S2D106	**RBM**	8.0	34.6	1-69 (97.2)	Hosp. (98)	Strong	Thomson et al.
S2D32	**RBM**	4.6	104.6	3-49 (98.3)	Hosp. (49)	Strong	Thomson et al.
S2N22	**RBM**	16.8	543.4	3-23 (96.5)	Hosp. (51)	Strong	Thomson et al.
S2D97	**RBM**	10.0	332.9	2-5 (96.9)	Hosp. (98)	Weak	Thomson et al.
S2H71	**RBM**	18.2	622.8	2-5 (99)	Sympt. (45)	Moderate	Thomson et al.
S2H70	**RBM**	194.9	10000.0	1-2 (99)	Sympt. (45)	Weak	Thomson et al.
S2X58	**RBM**	14.4	10000.0	1-46 (99)	Sympt. (48)	Strong	Thomson et al.
S2N12	**RBM**	10.6	10000.0	4-39 (97.6)	Hosp. (51)	Strong	Thomson et al.
S2X30	**RBM**	10.0	10000.0	1-69 (97.9)	Sympt. (48)	Strong	Thomson et al.
etesevimab	**RBM**	28.7	23.0 / 10.3*	3-66 (99.7)	Sympt. (?)	Strong	R. Shi et al. Nature 2020
casirivimab	**RBM**	6.0	7.2 / 3.5*	3-30 (98.6)	Immunized mice	Strong	J. Hansen et al. Science 2020
regdanvimab	**RBM**	2.2	29.2 / 16.3*	2-70 (?)	Sympt. (?)	Strong	
imdevimab	**RBM**	31.9	1607.2 / 45.4*	3-11 (98.6)	Sympt. (?)	Strong	J. Hansen et al.Science 2020
bamlanivimab	**RBM**	7.8	10000 / 10000*	1-69 (99.7)	Sympt. (?)	Strong	Jones et al.Sci Transl Med 2021
S309	**non-RBM**	63.9	46.4	1-18 (97.2)	SARS-CoV	Weak	Pinto et al.
S2X35	**non-RBM**	181.2	224.6	1-18 (98.6)	Sympt. (48)	Strong	Piccoli et al.
S2H94	**non-RBM**	134.1	182.9	3-23 (93.4)	Sympt. (81)	Strong	Thomson et al.
S2X259	**non-RBM**	74.2	101.1	1-69 (94.1)	Sympt. (75)	Moderate	Tortorici et al (BioRxiv 2021)
S2H97	**non-RBM**	599.3	1260.4	5-51 (98.3)	Sympt. (81)	Weak	Collier et al.; Starr et al (BioRxiv 21)
S2X609	**non-RBM**	19.7	10000.0	1-69 (93.8)	Sympt. (271)	Strong	Collier et al.
S2X608	**non-RBM**	18.9	10000.0	1-33 (93.2)	Sympt. (271)	Strong	Collier et al.
S2X619	**non-RBM**	18.2	10000.0	1-69 (92.7)	Sympt. (271)	Strong	Collier et al.
S2X305	**non-RBM**	11.8	9522.5	1-2 (95.1)	Sympt. (125)	Strong	Collier et al.

DSO, days after symptom onset. Sympt., symptomatic. Hosp., hospitalized. SARS-CoV, infected with SARS-CoV virus. *clinical-stage mAbs tested with Vero E6 cells not expressing TMPRSS2

Extended Data Table 3: Monoclonal antibodies used in neutralisation assays against pseudotyped virus bearing spike from WT (Wuhan-1 D614G) or B.1.617.2.

Extended Data Table 4A: Clusters of SARS-CoV-2 infections in three hospitals with near universal staff vaccination during first half of 2021.

	B.1.617.2 (N= 112)	Non-B.1.617.2 (N=20)	P value
Median age *years* (IQR)	36.5 (27.0-49.5)	32.5 (27.5-44.0)	0.56[a]
Female *%*	51.8 (58)	50.0 (10)	0.88[b]
Hospital *%*			
1	9.8 (11)	15.0 (3)	0.15[b]
2	53.6 (60)	30.0 (6)	
3	36.6 (41)	55.0 (11)	
Median Ct value (IQR)	22.5 (16.4-28.6)[c]	19.8 (17.3-22.8)	0.48
Number of vaccines doses %[†]			
0	10.8 (12)	35.0 (7)	0.005[b]
1	20.7 (23)	30.0 (6)	
2	68.5 (76)	35.0 (7)	
Hospitalised %*			
No	95.5 (64)	93.3 (14)	0.72[b]
Yes	4.5 (3)	6.7 (1)	
Anti-Spike IgG GMT (95% CI)	15.5 (4.6-52.9)[d]	29.5 (0.0-2.4x10^6)[e]	0.69[a]
Median Symptom duration *days*	1.5 (1.0-3.0)[f]	1.0 (1.0-2.0)[g]	0.66[a]

[a] Wilcoxon rank-sum test. [b]Chi square test. [c]111 of 112 available. [d]11 of 112. [e]2 of 20. [f]63 of 112. [g] 12 of 20. [†]Vaccine status missing for 1 of 132. *Hospitalisation data is unavailable from Hospital 1. IQR- inrerquartile range, GMT- geometric mean titre. CI- confidence interval.

Extended Data Table 4B: **Relative ChAdOx-1 vaccine efficacy against B1.617.2 v non-B1.617.2:** Odds ratios for detection of B.1.617.2 relative to non-B.1.617.2 in vaccinated compared to unvaccinated individuals

	B1.617.2	Non-B.1.617.2	B1.617.2: Non-B.1.617.2	OR (95% CI)	P value	aOR (95% CI)	P value
Unvaccinated	12	7	1.71	-		-	
Vaccinated							
Dose 1	23	6	3.83	2.24 (0.61-8.16)	0.22	2.06 (0.51-8.40)	0.31
Dose 2	76	7	10.86	6.33 (1.89-21.27)	0.003	5.14 (1.32-20.0)	0.018
Dose 1 and 2	99	13	7.62	4.44 (1.48-13.30)	0.008	3.59 (1.06-12.16)	0.04

OR; odds ratio aOR; Adjusted odds ratio.

Supplementary Material: Semi-Mechanistic SARS-CoV-2 Transmission Model

1 Model description

The model described here builds on a previously published model of SARS-CoV-2 transmission introduced in Flaxman et al, 2020 [1], subsequently extended into a two-category framework in Faria et al [2], 2020 to describe and characterise the dynamics of the Gamma variant in Manaus, Brazil. Replication code is available at `https://github.com/ImperialCollegeLondon/delta_modelling`.

In brief, the model describes two categories, denoted $s \in \{1, 2\}$. In our setting, category 2 is the Delta variant, and category 1 is a group for all other variants in circulation (wild type, Alpha, Beta, etc.). The reproduction number for the first category (before adjusting for susceptible depletion) is modelled as

$$R_{s=1,t} = \mu_0 \, 2 \, \sigma(X_t) \, , \tag{1}$$

where μ_0 is a scale parameter (3.3), σ is the logistic function, and X_t is a second-order autoregressive process with weekly time innovations, as specified in Unwin et al, 2020 [3]. X_t therefore models R as a flexible differential function. The reproduction number for the second category is modelled as

$$R_{s=2,t} = \rho \mathbf{1}_{[t_2,\infty)} R_{1,t} \, , \tag{2}$$

with

$$\rho \sim \text{Gamma}(5, 5) \, \in [0, \infty) \, , \tag{3}$$

where ρ is a parameter defining the relative transmissibility of category 2 compared to category 1, t_2 is the date of emergence of category 2, and $\mathbf{1}_{[t_2,\infty)}$ is an indicator function taking the value of 0 prior to t_2, and 1 thereafter, highlighting that category 2 does not contribute to the observed epidemic evolution before its emergence.

Infections arise for each category according to a discrete renewal process [4] with susceptible depletion

$$i_{s,t} = \left(1 - \frac{n_{s,t}}{N}\right) R_{s,t} \sum_{\tau<t} i_{s,\tau} g_{t-\tau} \, , \tag{4}$$

where N is the total population size, $n_{s,t}$ is the total extent of population immunity to category s present at time t, and g is the generation interval distribution.

The susceptible depletion term for category s is modelled as

$$n_{s,t} = \sum_{\tau<t} i_{s,\tau} W_{t-\tau} + \beta_s \left(1 - \alpha_{s,t}\right) \sum_{\tau<t} i_{\setminus s,\tau} W_{t-\tau} \, . \tag{5}$$

under the assumption of symmetric cross-immunity between categories 1 and 2 with prior on the cross-immunity

$$\beta \sim \text{Beta}(2, 1)\,. \tag{6}$$

$W_{t-\tau}$ is the time-dependent waning of immunity elicited by previous infection, which is modelled as a Rayleigh survival-type function with Rayleigh parameter of $\sigma = 310$, for which 50% of individuals are immune to reinfection by the same category after 1 year. The cross-immunity susceptible term $\alpha_{s,t}$ is modelled as

$$\alpha_{s,t} = \frac{(1-\beta_s)\sum_{\tau<t} i_{s,\tau} W_{t-\tau}}{N - \beta_s \sum_{\tau<t} i_{s,\tau} W_{t-\tau}}\,. \tag{7}$$

Infections of category 1 are seeded for six days at the start of the epidemic as

$$i_{1,t_{1..6}} \sim \text{Exponential}(1/\tau), \tag{8}$$

with

$$\tau \sim \text{Exponential}(0.03)\,, \tag{9}$$

Infections of category 2 are seeded for one day only, the date of introduction t_2, as

$$i_{2,t_2} \sim \text{Normal}(0, 20^2)\ \in [1, \infty)\,. \tag{10}$$

Non-unit seeding of category 2 and the diffuse prior represent our uncertainty in the precise date and magnitude of category 2's introduction/importation.

The model generates deaths via the following mechanistic relationship:

$$d_t = \sum_s \text{ifr}_s \sum_{\tau<t} i_{s,\tau}\pi_{t-\tau}\,. \tag{11}$$

The infection fatality ratios (ifr_s) of each of the categories are given moderately informative priors:

$$\text{ifr}_s \sim \text{Normal}(0.3, 0.02^2)\ \in [0, 100] \tag{12}$$

with our central estimate based on the results of Brazeau et al [5] and adjusted for the demography of the city. We allow for some potential variation around this estimate however, with the prior providing some support for IFRs in the range 0.25% - 0.35%. A limitation of the model is the assumption of homogeneous exposure across subsets of the population.

The observation model uses three types of data from four sources.

Likelihood component 1. The likelihood for the expected deaths D_t is modelled with a negative binomial distribution,

$$D_t \sim \text{NegativeBinomial}(d_t(1-\omega), d_t + \frac{d_t^2}{\phi})\,, \tag{13}$$

with mortality data d_t, dispersion prior

$$\phi \sim \text{Normal}(0, 5)\ \in [0, \infty)\,. \tag{14}$$

and undereporting factor ω, which describes the degree of death underascertainment, e.g. a value of 0.25 means 25% of COVID-19 deaths are not reported (due, e.g. to limited testing).

Likelihood component 2. Genomic data from individuals, where infections were sequenced and where the sequence was uploaded to GISAID, is modelled with a Binomial likelihood for the proportion of sequenced genomes identified as categories 1 and 2 at time t:

$$G_t^+ \sim \text{Binomial}(G_t^1 + G_t^2, \theta_t)\,, \tag{15}$$

with counts for category i denoted G_t^i. The success probability for category 2 is modelled as the infection ratio

$$\theta_t = \frac{\tilde{i}_{2,t}}{\tilde{i}_{1,t} + \tilde{i}_{2,t}}\,, \tag{16}$$

where $\tilde{i}_{s,t}$ is given by

$$\tilde{i}_{s,t} = \sum_{\tau \leq t} i_{s,\tau}\, \kappa_{t-\tau}\,, \tag{17}$$

to account for the time varying PCR positivity displayed over the natural course of a COVID-19 infection. The distribution κ describes the probability of being PCR positive over time following infection, and is based on [6].

Likelihood component 3.

Serological data from two sources are incorporated in our modelling framework. The observed seropositivity (S_t) on a given day, t, is modelled as follows

$$S_t \sim \text{Normal}(\sum_{\tau \leq t} i_{s,\tau} C_{t-\tau}, \sigma_s)\,, \tag{18}$$

where $C_{t-\tau}$ is the cumulative probability of an individual infected on day τ having seroconverted by time t. This distribution is empirical and based on [7]. The σ_s is given a Gamma$(5, 1)$ prior.

Eq (4) can be modified to account for population effects (decreasing susceptible population over time) such that no over-shooting happens due to discretization as follows [8, 9]:

$$i_{s,t} = (N - n_{s,t}) \left(1 - \exp\left(-\frac{i_{s,t}}{N}\right)\right), \tag{19}$$

The formula for $i_{s,t}$ is derived from a continuous time model on $[t-1, t]$. This is to avoid discrete time effects such as infections going above the total population N. Specifically, we assume that the infections $i(\Delta t)$ in $[t-1, t-1+\Delta t]$ are given by the differential equation $\partial i(\Delta t)/\partial \Delta t = i_t(1 - (n_{s,t} + i(\Delta t))/N)$, which has the solution $i(1) = i_t$ as above.

Model Running and Inference Parameter inference was carried out using the probabilistic programming language Stan [10], using an adaptive Hamiltonian Monte Carlo (HMC) sampler and implemented in RStan version 2.11 (R version 4.04). We ran 3 chains for 1000 iterations, with 500 iterations of warmup, to obtain a total of 1500 posterior samples which were used for subsequent inference and statistical analysis. Posterior convergence was assessed using the Rhat statistic (all of which were below 1.01) and by diagnosing divergent transitions of the HMC sampler.

2 Simulations

Using a simulation approach, we now assess whether our model can correctly recover the ground truth values for altered epidemiological characteristics, specifically changes in immune evasion and / or transmissibility. We use our model to simulate synthetic epidemics, keeping the start date for delta as 31st Jan 2021, ifr as 0.3% and 0.32% for non-delta and delta-strain respectively. We simulate two separate scenarios: A) with no chance of immune evasion and transmisssibility increase of $1.8x$, and B) with 50% chance of immune evasion and transmisssibility increase of $1.6x$. Simulated datasets and replication code are provided in the GitHub repository `http://github.com/ImperialCollegeLondon/delta_modelling`.

Ideally, fitting the model to synthetic data should succeed in correctly recovering the epidemiological quantities of interest; this sanity check gives us confidence that the model will be able to recover "ground truth" epidemiological characteristics when fit to real data, as in the main modeling analysis of the paper. The results are shown in Figure 1—the posterior mean estimates from the fitted model (red circles) recover the values used for the simulation (black circles), supporting the appropriateness of our modeling choices.

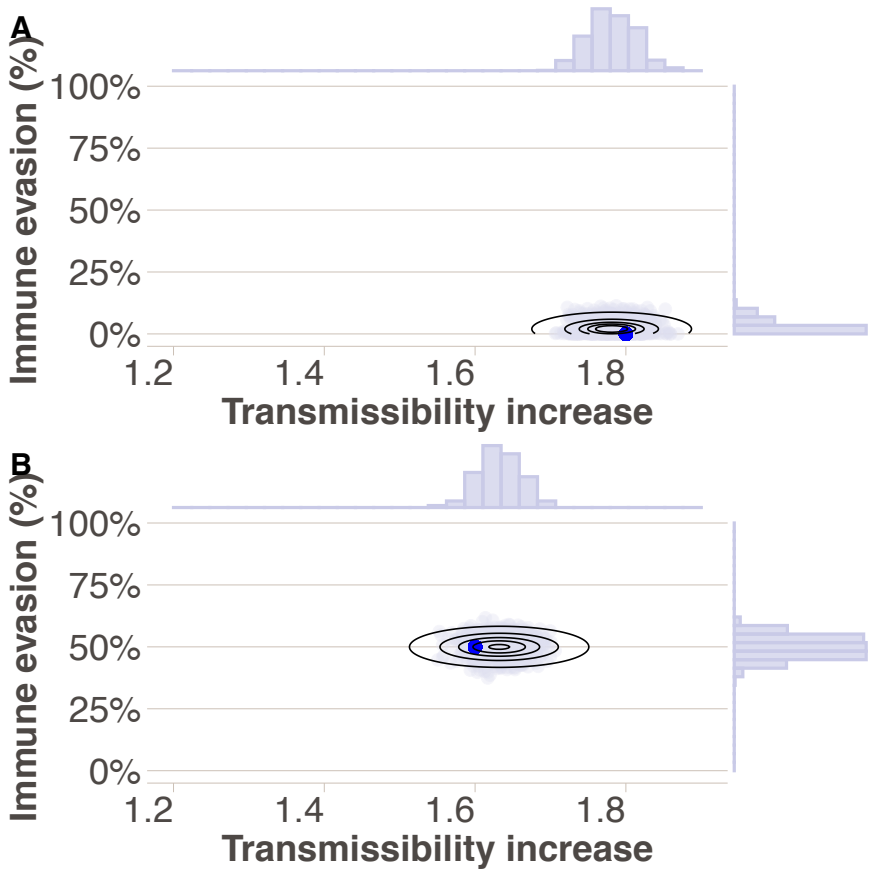

Figure 1: Estimated values for epidemiological characteristics from simulated data settings. Ground truth is indicated by black circles for (A) no immune evasion, increased transmissibility of 1.8x and (B) 50% immune evasion, increased transmissibility of 1.6x. In both (A) and (B), the ground truth blue circles, are well within the Bayesian 95% credible intervals (Black contours refer to posterior density intervals ranging from the 95% and 5% isoclines).

References

[1] Seth Flaxman, Swapnil Mishra, Axel Gandy, H Juliette T Unwin, Thomas A Mellan, Helen Coupland, Charles Whittaker, Harrison Zhu, Tresnia Berah, Jeffrey W Eaton, et al. "Estimating the effects of non-pharmaceutical interventions on COVID-19 in Europe". In: *Nature* 584.7820 (2020), pp. 257–261. DOI: https://doi.org/10.1038/s41586-020-2405-7.

[2] Nuno R Faria, Thomas A Mellan, Charles Whittaker, Ingra M Claro, Darlan da S Candido, Swapnil Mishra, Myuki A E Crispim, Flavia C S Sales, Iwona Hawryluk, John T McCrone, Ruben J G Hulswit, Lucas A M Franco, Mariana S Ramundo, Jaqueline G de Jesus, Pamela S Andrade, Thais M Coletti, Giulia M Ferreira, Camila A M Silva, Erika R Manuli, Rafael H M Pereira, Pedro S Peixoto, Moritz U G Kraemer, Nelson Gaburo Jr, Cecilia da C Camilo, Henrique Hoeltgebaum, William M Souza, Esmenia C Rocha, Leandro M de Souza, Mariana C de Pinho, Leonardo J T Araujo, Frederico S V Malta, Aline B de Lima, Joice do P Silva, Danielle A G Zauli, Alessandro C de S Ferreira, Ricardo P Schnekenberg, Daniel J Laydon, Patrick G T Walker, Hannah M Schlüter, Ana L P Dos Santos, Maria S Vidal, Valentina S Del Caro, Rosinaldo M F Filho, Helem M Dos Santos, Renato S Aguiar, José L Proença-Modena, Bruce Nelson, James A Hay, Mélodie Monod, Xenia Miscouridou, Helen Coupland, Raphael Sonabend, Michaela Vollmer, Axel Gandy, Carlos A Prete Jr, Vitor H Nascimento, Marc A Suchard, Thomas A Bowden, Sergei L K Pond, Chieh-Hsi Wu, Oliver Ratmann, Neil M Ferguson, Christopher Dye, Nick J Loman, Philippe Lemey, Andrew Rambaut, Nelson A Fraiji, Maria do P S S Carvalho, Oliver G Pybus, Seth Flaxman, Samir Bhatt, and Ester C Sabino. "Genomics and epidemiology of the P.1 SARS-CoV-2 lineage in Manaus, Brazil". en. In: *Science* (Apr. 2021).

[3] H Juliette T Unwin, Swapnil Mishra, Valerie C Bradley, Axel Gandy, Thomas A Mellan, Helen Coupland, Jonathan Ish-Horowicz, Michaela AC Vollmer, Charles Whittaker, Sarah L Filippi, et al. "State-level tracking of COVID-19 in the United States". In: *Nature communications* 11.1 (2020), pp. 1–9.

[4] Willy Feller. "On the Integral Equation of Renewal Theory". In: *The Annals of Mathematical Statistics* (1941). ISSN: 0003-4851. DOI: 10.1214/aoms/1177731708.

[5] Nicholas Brazeau, Robert Verity, Sara Jenks, Han Fu, Charles Whittaker, Peter Winskill, Ilaria Dorigatti, Patrick Walker, Steven Riley, Ricardo P Schnekenberg, et al. "Report 34: COVID-19 infection fatality ratio: estimates from seroprevalence". In: (2020). URL: https://www.imperial.ac.uk/mrc-global-infectious-disease-analysis/covid-19/report-34-ifr/.

[6] Joel Hellewell, Timothy William Russell, Rupert Beale, Gavin Kelly, Catherine Houlihan, Eleni Nastouli, Adam J Kucharski, SAFER Investigators, Field Study Team, Crick COVID-19 Consortium, et al. "Estimating the effectiveness of routine asymptomatic PCR testing at different frequencies for the detection of SARS-CoV-2 infections". In: *medRxiv* (2020). DOI: https://doi.org/10.1101/2020.11.24.20229948.

[7] Benny Borremans, Amandine Gamble, KC Prager, Sarah K Helman, Abby M McClain, Caitlin Cox, Van Savage, and James O Lloyd-Smith. "Quantifying antibody kinetics and RNA detection during early-phase SARS-CoV-2 infection by time since symptom onset". In: *Elife* 9 (2020), e60122. DOI: 10.7554/eLife.60122.

[8] James A. Scott, Axel Gandy, Swapnil Mishra, Juliette Unwin, Seth Flaxman, and Samir Bhatt. *epidemia: Modeling of Epidemics using Hierarchical Bayesian Models*. R package version 0.5.3. 2020. URL: https://imperialcollegelondon.github.io/epidemia/.

[9] Samir Bhatt, Neil Ferguson, Seth Flaxman, Axel Gandy, Swapnil Mishra, and James A. Scott. "Semi-Mechanistic Bayesian Modeling of COVID-19 with Renewal Processes". In: *arXiv* (2020). eprint: 2012.00394.

[10] Andrew Gelman Matthew D. Hoffman Daniel Lee Ben Goodrich Michael Betancourt Marcus Brubaker Jiqiang Guo Peter Li Carpenter Bob and Allen Riddell. "Stan: A probabilistic programming language." In: *Journal of statistical software* (2017).